University of Tennessee, Knoxville
TRACE: Tennessee Research and Creative Exchange

Masters Theses | Graduate School

5-2003

Design of a Piezoelectric Actuator Using Topology Optimization

Joachim Drenckhan
University of Tennessee - Knoxville

Follow this and additional works at: https://trace.tennessee.edu/utk_gradthes

 Part of the Aerospace Engineering Commons

Recommended Citation

Drenckhan, Joachim, "Design of a Piezoelectric Actuator Using Topology Optimization. " Master's Thesis, University of Tennessee, 2003.
https://trace.tennessee.edu/utk_gradthes/1936

This Thesis is brought to you for free and open access by the Graduate School at TRACE: Tennessee Research and Creative Exchange. It has been accepted for inclusion in Masters Theses by an authorized administrator of TRACE: Tennessee Research and Creative Exchange. For more information, please contact trace@utk.edu.

To the Graduate Council:

I am submitting herewith a thesis written by Joachim Drenckhan entitled "Design of a Piezoelectric Actuator Using Topology Optimization." I have examined the final electronic copy of this thesis for form and content and recommend that it be accepted in partial fulfillment of the requirements for the degree of Master of Science, with a major in Aerospace Engineering.

Arnold Lumsdaine, Major Professor

We have read this thesis and recommend its acceptance:

J.A.M Boulet, Frank H. Speckhart, Charles Collins

Accepted for the Council:
Carolyn R. Hodges

Vice Provost and Dean of the Graduate School

(Original signatures are on file with official student records.)

To the Graduate Council:

I am submitting herewith a thesis written by Joachim Drenckhan entitled "Design of a piezoelectric actuator using topology optimization." I have examined the final electronic copy of this thesis for form and content and recommend that it be accepted in partial fulfillment of the requirements for the degree of Master of Science, with a major in Aerospace Engineering.

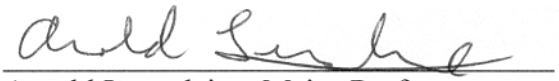

Arnold Lumsdaine, Major Professor

We have read this thesis
and recommend its acceptance:

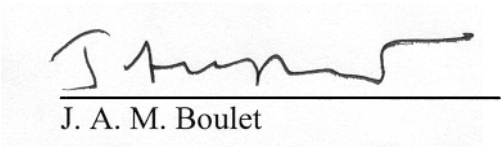

J. A. M. Boulet

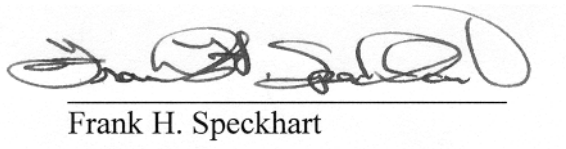

Frank H. Speckhart

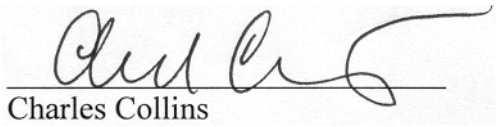

Charles Collins

Accepted for the Council:

Anne Mayhew
Vice Provost and Dean of Graduate Studies

(Original signatures are on file with official student records.)

Design of a piezoelectric actuator using topology optimization

A Thesis
Presented for the
Master of Science
Degree
The University of Tennessee

Joachim Drenckhan

May 2003

Acknowledgments

I wish to thank all those who helped me in completing my Master of Science in Aerospace Engineering. Special thanks go to Dr. Lumsdaine without his input, motivation and knowledge this work would not have been possible. He has been a great professor, mentor and adviser. I thank my committee members Dr. Boulet, Dr. Speckhart and Dr. Collins for being in my committee.

I thank my girlfriend Astrid Gämlich for supporting me mentally and enduring that I was gone for a long time.

Abstract

This study investigates the optimal topology for a piezoelectric actuator under a static load.

The project consists of two major parts: implementation of the control law into the commercial finite element code ABAQUS and studies in topology optimization. The first part gives a thorough derivation and explanation of the implementation of static feedback control and dynamic proportional and derivative control. The result is compared with results published in the literature. The second part examines the results of topology optimization with different geometries and constraints. Thus, this study develops fundamental understanding of advantageous shapes for optimal performing piezoelectric actuators.

Table of Contents

List of Tables

List of Figures

Nomenclature

A	Amplitude, Area
C	Capacitance
D_{ijkl}	Mechanical constitutive tensor
E_j	Electric field
F	Mechanical force vector
$F(x)$	Objective function
G_d	Derivative gain matrix
G_p	Proportional gain matrix
I	Identity matrix
K_{uu}	Mechanical stiffness matrix
$K_{u\Phi}$	Piezoelectric coupling matrix
$K_{\Phi\Phi}$	Dielectric matrix
L	Length
M	Mass matrix
M_0	Applied Moment
P_c	Control Force
Q	Nodal electric charge vector
U	Nodal displacement vector
V	Volume

b	Width
e_{ijk}	Piezoelectric coupling coefficient tensor
h	Height
h_i	Equality constraint
g_i	Inequality constraint
h	Thickness
p_{ij}	Dielectric tensor
q_i	Electric displacement vector
r	Radius
u	Displacement
x	Design variable

Greek Symbols

q	Angle
Φ	Nodal electric potential vector
a	Rayleigh damping factor
b	Rayleigh damping factor
d	Difference, Deflection
e_{ij}	Strain tensor
h	Loss factor
m	Poisson’s ratio

r	Material density, Distance to neutral axis
s_{ij}	Stress tensor
w	Frequency

Superscripts

a	Actuator
b	Beam
max	Maximum
s	Sensor

Subscripts

C	Compression
HB	Half power bandwidth
T	Tension
ave	Averaged
eq	Equivalent
n	Natural frequency
out	Output point
1,2,3,..,n	Node number

1 INTRODUCTION

Piezoelectric materials have the unique capability of producing mechanical strain when subjected to an electric potential or, conversely, of generating an electrical charge when subjected to mechanical strain. This capability has been used in active control systems utilizing piezoelectric elements as actuating and sensing devices (Tzou and Tseng 1990). The research done in this area has demonstrated that piezoelectric materials have the ability to modify the static and dynamic characteristics of structures. The stiffness and damping characteristics of a structure can be modified by the application and control of piezoelectric materials. Piezoelectric actuators have many unique characteristics that distinguish them from other actuators. A piezoelectric material exited with an activation voltage to induce a strain upon a structure is referred to as a piezoelectric actuator. Several of the favorable characteristics of piezoelectric actuators are that they can be formed to specific shapes and are relatively easy to control and to install. Therefore, piezoelectric actuators have favorable characteristics that make them a good choice for use in composite structures where they can be easily installed.

One of the disadvantages of piezoelectric materials is that they produce very little strain. Larger strains would increase the performance of the piezoelectric actuator characteristics and is therefore desirable. For this reason various research attempts have been made to modify the microstructure of the piezoelectric material to increase strain (Silva, Nishiwaki et al. 2000). However, very little research has been done in detecting the optimal shape of piezoelectric material to reduce displacement or maximize the damping characteristics of a mechanical structure. Topology optimization using

homogenization has been used in various areas of structural design and has been shown to be a good method for solving this kind of problem. For this reason, it is the purpose of the study to conduct a topology optimization for a piezoelectric actuator.

In this study, the objective is to determine the best topology of a piezoelectric actuator for a cantilever beam under a concentrated static load at the tip. This is done by conducting a topology optimization of the actuator. A parameter study is conducted with different material densities and different gains for the actuator. The results are compared and a "best" topology for this problem is determined.

Furthermore, attempts have been made to implement dynamic proportional and derivative control for active vibration damping.

1.1 LITERATURE REVIEW

A review of related papers is given to show the current state of research in this area. The introduced papers are divided into two major groups, describing (1) the finite element modeling of piezoelectric material and implementing a control law and (2) the topology optimization including approaches using piezoelectric elements.

1.1.1 FINITE ELEMENT MODELING AND CONTROL

Mechanical and electrical constitutive laws for piezoelectric materials have been well defined. Some commercial finite element codes already have the capability to use such elements, such as ABAQUS (Hibbit, Karlsson *et al.* 2002), which has been used for

this study. A good overview of the general topic of modeling piezoelectric materials in a finite element model has be done by Naillon *et al.* (1983), who describe a method to analyze piezoelectric structures by using the finite element method. Further work has been done by Lerch (1990), who expanded the finite element theory for piezoelectric materials to be used in two or three dimensions. Furthermore, Hossack *et al*. (1991) describes the finite element analysis of 1-3 transducers for different piezoelectric materials and compares the results with experiments. Another approach is shown by Guyan (1965), who removed the electrical degrees of freedom by using a condensation matrix. The control is applied over the remaining translational and rotational degrees of freedom.

Much research has been done in implementing control laws for piezoelectric materials to be used as sensors and actuators in smart materials. Tzou and Tseng (1990; 1991) describe a distributed piezoelectric sensor/actuator design for piezoelectric materials by using a finite element approach. Tzou (1993) has also done a more thorough derivation of the theory of piezoelectric material and its control in his book "Piezoelectric Shells." Ha *et al.* (1992) did a finite element analysis of structures containing piezoceramic sensors and actuators and compared the computational results with experiments. Similar research has been done by Baz and Ro (1995) who examined the performance characteristics of active constrained layer damping using piezoelectric and viscoeleastic materials by a finite element method and compared the results to experimental values. Valey and Rao (1996) built on these results to make a comparison of active, passive and hybrid damping in structural design. Vardan *et al*. (1996) describes

the closed loop finite element modeling of active damping in active structural vibration control. In the same area two papers have been published by Kim *et al.* (1996; 1997) which also describe the finite element modeling of smart structures including piezoelectric materials. The vibration and actuation characteristics of structures with a piezo-ceramic actuator have been examined by Han (1999) and compared with experimental results.

Other research has been done in the area of finding the best controller for smart structures. Since this is not the emphasis of this work, just a few publications are described. Gaudenzi *et al.* (2000) compares the control of beam vibrations between numerical and experimental results. A more thorough approach is taken by Gabbert *et al.* (2002) who examine the controller design for smart structures. Chang *et al*. (2002) describe how to design a robust vibration controller for a smart panel, also by using the finite element method.

1.1.2 TOPOLOGY OPTIMIZATION

Topology optimization is a relatively recent field and has been shown to be a good method for finding optimal topologies for structural problems with given boundary conditions. Bendsøe and Kikuchi (1988) first introduced the homogenization method for finding the optimal topology for a structural problem. A more thorough description of topology optimization using homogenization is given in the books by Hassani and Hinton (1999), Allaire (2002) and Bendsøe and Sigmund (2003).

Topology optimization has been applied in studies by Yi et al. (2000) who used topology optimization to optimize the shape of visoelastic materials to achieve best damping characteristics. Lumsdaine (2002) did similar work by using topology optimization for finding the best shape of constrained layer damping materials.

The idea of finding the best topology for a given problem has further been applied for smart materials, including piezoelectric materials. Some research has been done in using topology optimization for designing a piezo-composite microstructure to improve the piezoelectric sensor and actuator attributes. In this area, Silva *et al.* has to be mentioned, who published a verity of papers to this topic (Silva, Fonseca et al. 1997; Silva, Fonseca et al. 1998; Silva, Fonseca et al. 1999; Silva and Kikuchi 1999; Silva, Nishiwaki et al. 1999; Silva, Nishiwaki et al. 2000). Buehler *et al.* (2002) used topology optimization and homogenization on piezoelectric sensors to reduce the deflection of a cantilever beam made of piezoelectric material. Furthermore, a comparison of amplified piezoelectric actuators based on topology optimization has been done by Loveday (2002).

To the author's knowledge no previous study has been done in finding the optimal topology for a piezoelectric actuator of a beam under bending.

1.2 PROBLEM STATEMENT

The objective of this study is to determine the best topology of a piezoelectric actuator for a cantilever beam under a static load to minimize the deflection of the beam at the free end. The beam consists of three layers of material, a piezoelectric sensor, an

elastic beam and a piezoelectric actuator (figure 1.1). To determine the best topology of the actuator layer, a numerical optimization is conducted. Finite elements are typically used for topology optimization problems, as analytic formulations would be far too complex to use practically. Thus, the beam is modeled using finite elements with two-dimensional first-order continuum elements. Analysis is done using the commercial finite element code ABAQUS. A feedback control loop is implemented in the finite element model by modifying the stiffness matrices using MATLAB. The developed finite element model is linked with the commercial optimization algorithm VisualDoc by using a sequential linear programming algorithm (SLP). Parameter studies have been conducted by varying the number of elements and the total allowed amount of material in the actuator layer. The results of optimization with different geometries and feedback gains are shown.

Chapter two gives an overview of the finite element modeling and implementation of the feedback control loop in the commercial finite element code ABAQUS. Verification calculations and comparisons to published results have been made to confirm the correct implementation of the control law. Attempts have been made to implement dynamic proportional and derivative control for active vibration damping. Chapter three explains the basic idea of optimization and gives a detailed description of topology optimization using homogenization. The implementation of the finite element model in the optimization algorithm is described. Chapter four shows the results of the parameter study for different optimizations. The last chapter shows the conclusions of this work and gives an overview of possible future work.

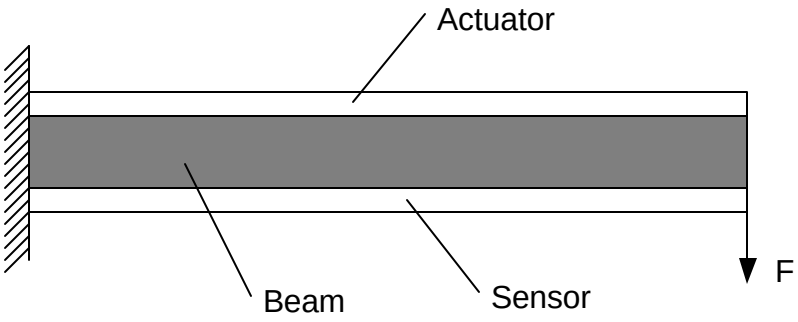

Figure 1.1 Modeled cantilever beam

2 FINITE ELEMENT FORMULATION

The goal of this study is to conduct a topology optimization for a mechanical system, which includes piezoelectric sensors and actuators. Since there is no reasonable analytical solution to this problem, a numerical representation needs to be determined. The finite element method has been chosen for this study, since it is widely available and is commonly used for topology optimization studies. For this reason, this Chapter gives an overview over the background of piezoelectric materials and their constitutive equations. Furthermore, the implementation of the control loop in the finite element model will be described for static and dynamic applications. Results of verification calculations of the implemented feedback control are shown at the end of the appropriate section. However, the derivation of the finite element formulation of piezoelectric materials will not be shown, since it has not been necessary for this research, as commercial software has been used for the finite element modeling. For details in the understanding the finite element formulation of piezoelectric materials please refer to Kim *et al.* (1997), Naillon *et al.* (1983) who give a good overview over this topic.

2.1 THEORY FOR PIEZOELCTRIC MATERIAL

Piezoelectricity is an electromechanical phenomenon that couples the elastic and electric fields. In general, a piezoelectric material responds to mechanical loads and generates an electric field. Conversely, an electric field applied to the material induces mechanical strains. Changes in temperature and ambient electric field are considered negligible. “These assumptions are compatible with the piezoelectric ceramics, polymers,

and composites in current use" (Silva, Fonseca et al. 1999) . For this reason, the constitutive relationship for piezoelectric materials can be written as:

$$s_{ij} = D_{ijkl} \cdot e_{kl} - e_{mij} \cdot E_m \tag{2.1}$$

$$q_i = e_{ijk} \cdot e_{jk} + p_{ij} \cdot E_j \tag{2.2}$$

where Equation 2.1 describes the relationship between the stresses (s_{ij}), the strains (e_{kl}) and the electric field (E_m), coupled through a fourth-order elastic tensor (D_{ijkl}) and a third-order piezoelectric tensor (e_{mij}). The piezoelectric tensor defines the coupling of the electric and elastic fields. The first index describes the direction of the electric field and the last two indices describe the direction of the elastic field. For example, the e_{211} field couples the electric filed in the 2-direction, with the elastic field in the 11-direction. This means, an applied electric field in the 2-direction results in strains in the 11-direction. Equation 2.2 describes the relationship between the electric displacement (q_i), the strains and the electric field, coupled through a third-order piezoelectric tensor and a second-order dielectric tensor (p_{ij}).

2.2 STATIC CALCULATION

The finite element equations for modeling a linear piezoelectric medium are described by Naillon *et al.* (1983) and Lerch (1990). For a static analysis, these equations can be written as:

$$\begin{bmatrix} K_{uu} & K_{u\Phi} \\ K_{\Phi u} & -K_{\Phi\Phi} \end{bmatrix} \begin{Bmatrix} U \\ \Phi \end{Bmatrix} = \begin{Bmatrix} F \\ Q \end{Bmatrix} \tag{2.3}$$

where K_{uu}, $K_{u\Phi}$ and $K_{\Phi\Phi}$ are the stiffness, piezoelectric and dielectric matrices, respectively. In some publications $K_{\Phi u}$ is described as $K_{u\Phi}^{t}$, which is identical. F, Q, U and Φ are the nodal mechanical force, the nodal electric charge, the nodal displacements and the nodal electric potential vectors, respectively. Both the sensor and the actuator can mathematically be described through equation 2.3. Sensor and actuator elements are herby denoted with a superscript 's' and 'a', respectively. Feedback control for the static case is applied through:

$$\{\Phi^{a}\} = [G_{p}] \cdot \{\Phi^{s}\} \tag{2.4}$$

where $[G_{p}]$ is a gain matrix the defines the magnitude of the gain for each actuator node. If equation 2.4 is insert into equation 2.3 for the actuator the following may be derived:

$$\begin{bmatrix} K_{uu}^{a} & K_{u\Phi}^{a} \\ K_{\Phi u}^{a} & -K_{\Phi\Phi}^{a} \end{bmatrix} \begin{Bmatrix} U^{a} \\ G_{p} \cdot \Phi^{s} \end{Bmatrix} = \begin{Bmatrix} F^{a} \\ Q^{a} \end{Bmatrix} \tag{2.5}$$

$$\begin{bmatrix} K_{uu}^{s} & K_{u\Phi}^{s} \\ K_{\Phi u}^{s} & -K_{\Phi\Phi}^{s} \end{bmatrix} \begin{Bmatrix} U^{s} \\ \Phi^{s} \end{Bmatrix} = \begin{Bmatrix} F^{s} \\ Q^{s} \end{Bmatrix} \tag{2.6}$$

Sensor and actuator equations can then be combined into:

$$\begin{bmatrix} K_{uu}^{s} & 0 & K_{u\Phi}^{s} & 0 \\ 0 & K_{uu}^{a} & K_{u\Phi}^{a} \cdot G_{p} & 0 \\ K_{\Phi u}^{s} & 0 & -K_{\Phi\Phi}^{s} & 0 \\ 0 & K_{\Phi u}^{a} & -K_{\Phi\Phi}^{a} \cdot G_{p} & 0 \end{bmatrix} \begin{Bmatrix} U^{s} \\ U^{a} \\ \Phi^{s} \\ \Phi^{a} \end{Bmatrix} = \begin{Bmatrix} F^{s} \\ F^{a} \\ Q^{s} \\ Q^{a} \end{Bmatrix} \tag{2.7}$$

This approach does not allow solving directly for the electric potential of the actuator nodes, since the fourth column is eliminated. If desired, the electric potentials of the actuator nodes can be recovered using equation 2.4.

For this work two generally different approaches of control have been used. The first approach applies a direct node-to-node control. This means, the electrical charge of a sensor node is directly applied to the corresponding actuator node. This approach is difficult to implement in reality. In most real systems the total electric potential of the sensor is applied to the actuator. Therefore, in a second approach the electrical charge of all sensor nodes is averaged and afterwards applied to all actuator nodes, which describes more commonly applied layer-to-layer control.

2.2.1 NODE-TO-NODE CONTROL

As mentioned above, node-to-node control applies the electrical charge of a sensor node directly to a corresponding actuator node. Figure 2.1 clarifies this method. In this study node-to-node control has been implemented in reading the stiffness matrices of each sensor and actuator element out of the commercial finite element program ABAQUS into MATLAB. Following the stiffness matrix, as described in equation 2.7, is assembled for one sensor and actuator element at a time. Finally, the new defined stiffness matrices are read back into ABAQUS and the complete system is also solved using ABAQUS.

2.2.2 LAYER-TO-LAYER CONTROL

Layer-to-layer control applies the total electric potential of the sensor to the actuator. This can be implemented in a finite element calculation by averaging the electrical charge of the senor nodes and applying this charge to the actuator nodes. This

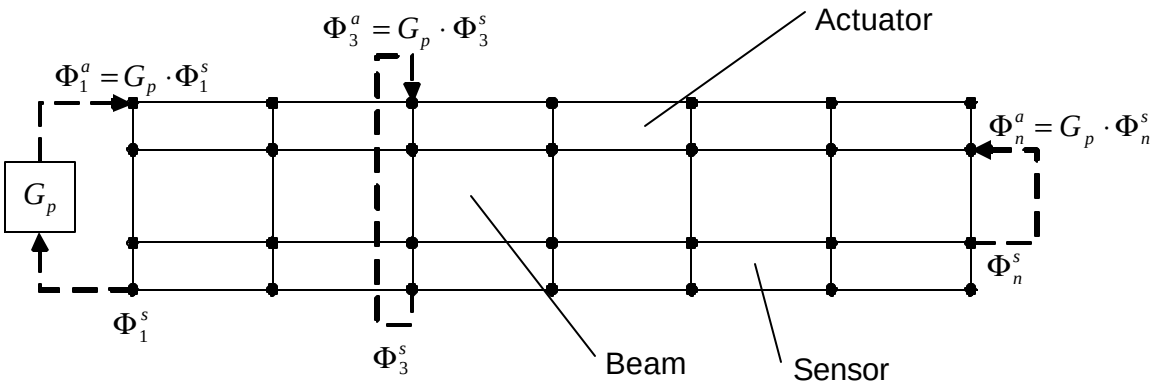

Figure 2.1 Node-to-Node control

has the effect that even in regions where there is no displacement of the sensor nodes, the corresponding actuator nodes will be loaded with an electrical charge. As mentioned above, this approach is more realistic, since in reality the measured electric potential is typically an average of the sensor over the sensor surface and the applied potential is applied evenly on the actuator surface.

To implement this type of control it is necessary to assemble the complete stiffness matrix for all actuator and sensor elements. This allows multiplying $K^a_{u\Phi}$ and $K^a_{\Phi\Phi}$ of the complete stiffness matrix with a gain matrix. The gain for node number one can be described as:

$$\Phi^a_1 = G_p \cdot \frac{\Phi^s_1 + \Phi^s_2 + \Phi^s_3 + ... + \Phi^s_n}{n} \tag{2.8}$$

where "n" describes the number of nodes at the surface where the electric potential is measured. From this consideration the gain matrix is concluded:

$$\begin{Bmatrix} \Phi^a_1 \\ \Phi^a_2 \\ \Phi^a_3 \\ \vdots \\ \Phi^a_n \end{Bmatrix} = \frac{G_p}{n} \begin{bmatrix} 1 & 1 & 1 & 1 & 1 & 1 & \cdots & 1 \\ 1 & 1 & 1 & 1 & 1 & 1 & \cdots & 1 \\ 1 & 1 & 1 & 1 & 1 & 1 & \cdots & 1 \\ \vdots & \vdots & \vdots & \vdots & \vdots & \vdots & \ddots & \vdots \\ 1 & 1 & 1 & 1 & 1 & 1 & \cdots & 1 \end{bmatrix} \begin{Bmatrix} \Phi^s_1 \\ \Phi^s_2 \\ \Phi^s_3 \\ \vdots \\ \Phi^s_n \end{Bmatrix} \tag{2.9}$$

Now the complete stiffness matrix can be assembled and the system can be solved.

2.2.3 IMPLEMENTATION FOR THE STATIC CASE

The implementation of the control law into the finite element code ABAQUS is done in three steps. First, the stiffness matrices are constructed in ABAQUS and written

to a file. In the next step, these matrices are read with MATLAB, and proportional control is applied in accordance to the theory described above. Following, the modified stiffness matrices are written out by MATLAB and read in by ABAQUS again, in which the final calculation is done. Figure 2.2 clarifies this procedure.

2.2.4 VERIFICATION FOR THE STATIC CASE

For a simple beam with a load only in the axial direction it is easily possible to derive an analytical result and compare the results with a finite element calculation. In order to validate the proportional control implementation a simple decoupled system has been modeled with geometry as shown in figure 2.3 and material properties as shown in table 2.1. Analytic results are then compared against results from the finite element calculation.

As described above the constitutive relationship for piezoelectric material is defined as:

$$s_{ij} = D_{ijkl} \cdot e_{kl} - e_{mij} \cdot E_m \tag{2.10}$$

$$q_i = e_{ijk} \cdot e_{jk} + p_{ij} \cdot E_j \tag{2.11}$$

For the one-dimensional case the equations reduce to:

$$s_{11} = D_{1111} \cdot e_{11} - e_{211} \cdot E_2 \tag{2.12}$$

$$q_2 = e_{211} \cdot e_{11} + p_{22} \cdot E_2 \tag{2.13}$$

The sensor has no electrical surface charge but is loaded with a force in the axial direction which leads to:

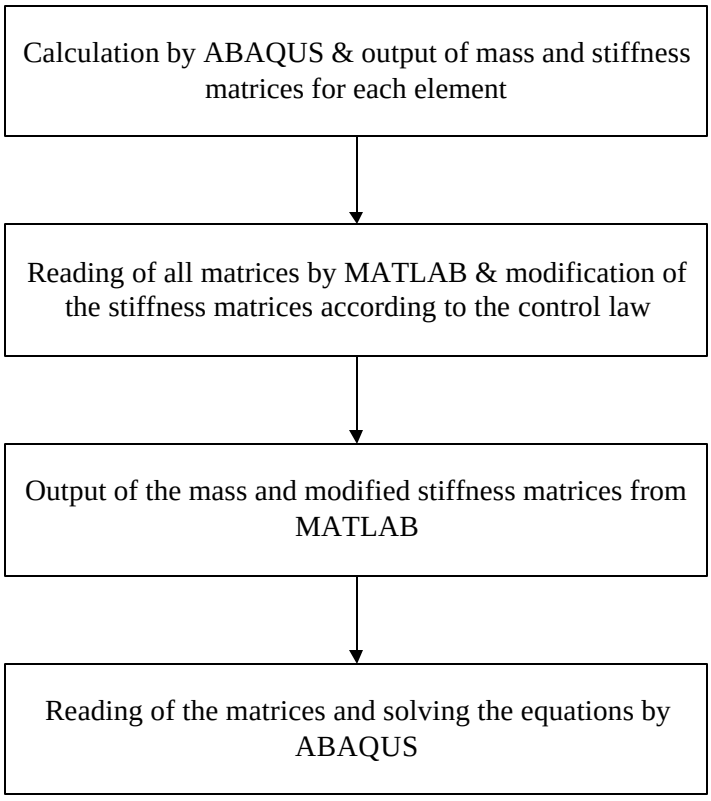

Figure 2.2 Process diagram for static control

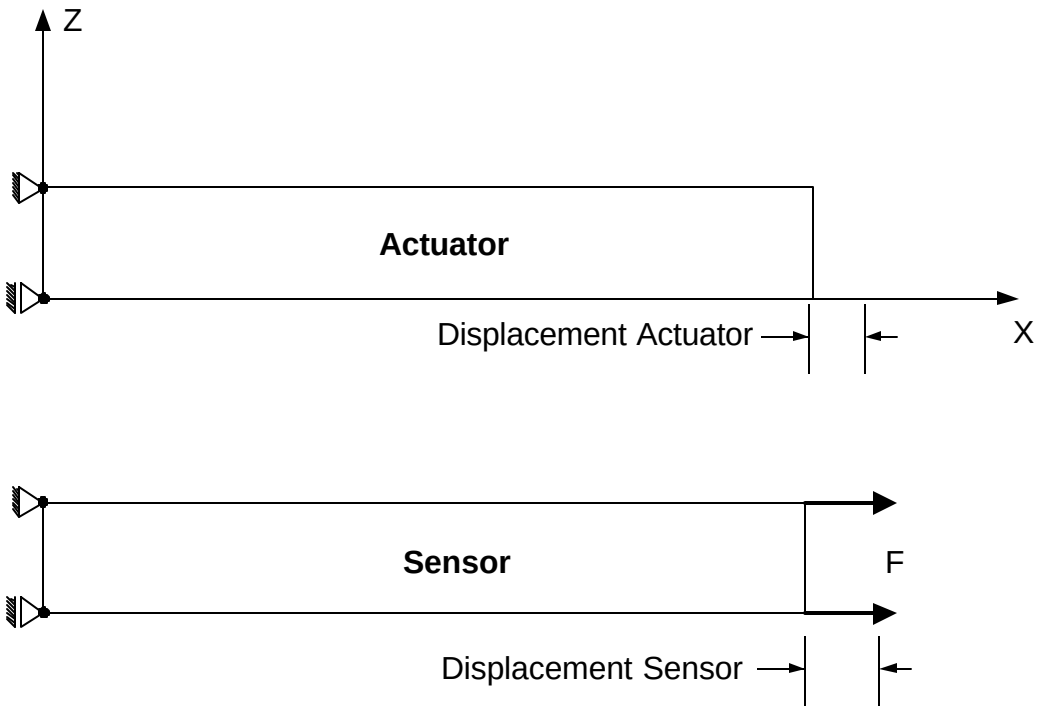

Figure 2.3 Decoupled beam system

Table 2.1 Material properties for simple decouple beam system

Material property	Value
Young's Modulus	$D^a_{1111} = D^s_{1111} = 20E8\ \frac{N}{m^2}$
Poisson's Ratio	$u = 0.3$
Piezoelectric stress coefficients	$e^a_{211} = e^s_{211} = 0.046\frac{C}{m^2}$
Dielectric constant	$p^a_{22} = p^s_{22} = 0.1041E-9\frac{F}{m}$
Length	$l^a = l^s = 0.1m$
Cross section area	$A^a = A^s = 0.01^2\ m^2$
Force	$F = 10\ N$
Gain	$G_p = 240$

$$s_{11}^{s} = \frac{F}{A} \tag{2.14}$$

$$q_2^s = 0 \tag{2.15}$$

Now, the electric field and the displacement in the x-direction of the sensor can be calculated as:

$$E_2^s = -\frac{s_{11}^{s} \cdot e_{211}^s}{e_{211}^s + p_{22}^s \cdot D_1^s} \tag{2.16}$$

$$e_{11}^s = \frac{s_{11}^{s} \cdot p_{22}^s}{e_{211}^s + p_{22}^s \cdot D_1^s} \tag{2.17}$$

The actuator is not loaded with a mechanical force and therefore

$$s_{11}^{a} = 0 \tag{2.18}$$

but an electric potential is applied to the actuator through the control law. This is defined in equation 2.4 as:

$$\{\Phi^a\} = [G_p] \cdot \{\Phi^s\} \tag{2.19}$$

which for the one-dimensional case results in:

$$E_2^a = G_p \cdot E_2^s \tag{2.20}$$

so that the strain of the actuator can be calculated as:

$$e_{11}^a = G_p \cdot E_2^s \left(\frac{e_{211}^a}{D_{1111}^a} + p_{22}^a \right) \tag{2.21}$$

The system shown in figure 2.3 has been modeled with ten elements for the actuator and sensor, respectively. The result of the finite element calculation has been checked against the theoretical values for both node-to-node and layer-to-layer control. The

implementation of the node-to-node control has furthermore been done with linear (four-noded) and quadratic (eight-noded) elements. The results of these calculations and computation time on a SUN UltraSPARC IIe are shown in table 2.2. As one can see, the results of the FEM calculation conform in all cases to one hundred percent with the theoretical values.

A second verification of the finite element calculation has been done by developing an analytic solution for a controlled piezoelectric cantilever beam loaded with a moment at the free end. The geometry and the properties of the beam are shown in figure 2.4 and table 2.3, respectively. For the development of the analytic solution the one-dimensional piezoelectric equations are considered again. This is a reasonable assumption, since the strain induced by the actuator in the axial direction is the main cause for the increased stiffness. Equations 2.12 and 2.13 are rewritten for the actuator and the sensor:

$$s_{11}^{a} = D_{1111}^{a} \cdot e_{11}^{a} - e_{211}^{a} \cdot E_{2}^{a} \tag{2.22}$$

$$q_{2}^{a} = e_{211}^{a} \cdot e_{11}^{a} + p_{22}^{a} \cdot E_{2}^{a} \tag{2.23}$$

$$s_{11}^{s} = D_{1111}^{s} \cdot e_{11}^{s} - e_{211}^{s} \cdot E_{2}^{s} \tag{2.24}$$

$$q_{2}^{s} = e_{211}^{s} \cdot e_{11}^{s} + p_{22}^{s} \cdot E_{2}^{s} \tag{2.25}$$

where s_{11}^{a}, s_{11}^{s}, e_{11}^{a}, e_{11}^{s}, E_{2}^{a}, E_{2}^{s} and q_{2}^{a} are all unknowns. Since no electrical charge is applied to the sensor:

$$q_{2}^{s} = 0 \tag{2.26}$$

The control law is applied as described before through:

$$\Phi^{a} = G_{p} \cdot \Phi^{s} \tag{2.27}$$

and can be restated through the definition of the surface charge density:

Table 2.2 Validation of static decoupled system

		Tip-Displacement Sensor [m]	Tip-Displacement Actuator [m]	Computation Time [sec]
Node-to-Node	Linear elements	4.9497E-6	-1.2073E-5	3.82
	Quadratic Elements	4.9497E-6	-1.2073E-5	4.56
Layer-to-Layer	Linear elements	4.9497E-6	-1.2073E-5	4.08
Theory		4.9497E-6	-1.2073E-5	--

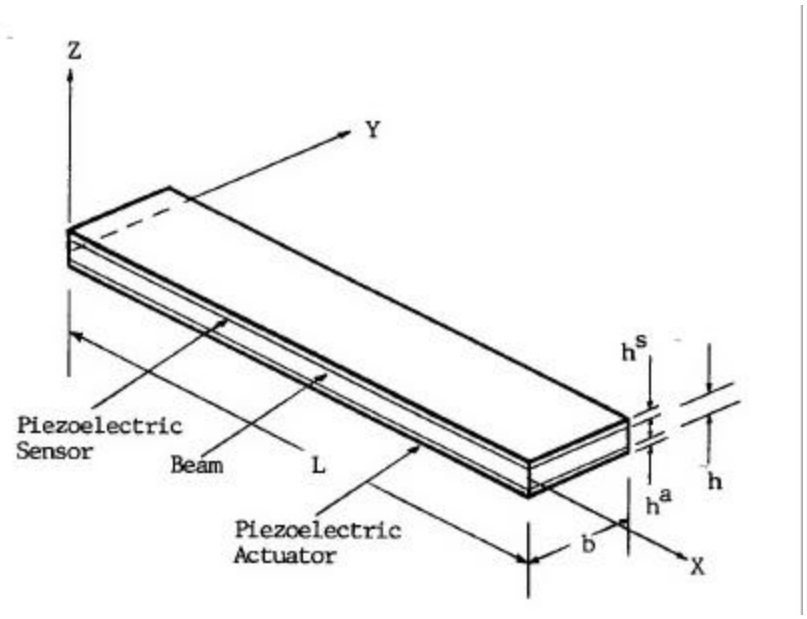

Figure 2.4 Tzou Beam

Table 2.3 Properties for the Tzou Beam (static case)

Plexiglas Beam	
Young's Modulus	$D = 3.1028 \cdot 10^{9} \frac{N}{m^2}$
Thickness	$h = 1.6 \cdot 10^{-3}\ m$
Width	$b = 0.01m$
Length	$L = 0.1m$
Poisson's ratio	$m = 0.3$
Sensor/Actuator Layer	
Young's Modulus	$D^s = D^a = 2.00 \cdot 10^{9} \frac{N}{m^2}$
Sensor/Actuator thickness	$h^a = h^s = 40mm$
Dielectric constant	$p^a = p^s = 1.06481 \cdot 10^{-10} \frac{F}{m}$
Piezoelectric constant	$e^a_{311} = e^s_{311} = 0.046 \frac{V\,m}{N}$

$$q_2^a = \frac{Q_2^a}{A^a} = \frac{C \cdot \Phi^a}{A^a} = G_p \frac{C \cdot \Phi^s}{A^a} \tag{2.28}$$

where Q_2^a is the electrical charge of the actuator and C is the capacitance, respectively. The capacitance can be written as:

$$C = \frac{p_{22} \cdot A}{h} \tag{2.29}$$

where h is the distance between the applied electric potentials. Now equations 2.28 and 2.29 can be combined into:

$$q_2^a = G_p \cdot p_{22}^a \cdot E_2^a \tag{2.30}$$

which is used to apply the control law for the analytic solution.

Since not enough equations are available to solve this system more equations need to be developed. The sensor and actuator layer are small compared to the beam layer and it can be assumed that the stresses in the actuator and sensor layer are constant For this reason the sum of forces in the x-direction is calculated (figure 2.5).

$$\begin{aligned}
&\sum F_x = 0 \\
&\Rightarrow \int_A s \; dA = -P_c \\
&\Rightarrow \int_{A^a} s \; dA + \int_{A^b} s \; dA + \int_{A^s} s \; dA = -Pc \\
&\Rightarrow s_{11}^a \cdot A^a + \int_0^{h-r} \frac{s_{\max T}^b}{h-r} \cdot z \, dA - \int_0^r \frac{s_{\max C}^b}{r} \cdot z \, dA + s_{11}^s \cdot A^s = -P_c \\
&\Rightarrow s_{11}^a \cdot A^a + \frac{1}{2} \cdot s_{\max T}^b \cdot b \cdot (h-r) - \frac{1}{2} \cdot s_{\max C}^b \cdot b \cdot r + s_{11}^s \cdot A^s = -P_c
\end{aligned} \tag{2.31}$$

A new variable r is introduced, which measures the distance from the top of the beam to the neutral axis. This is necessary, since the location of the neutral axis changes by applying a control force.

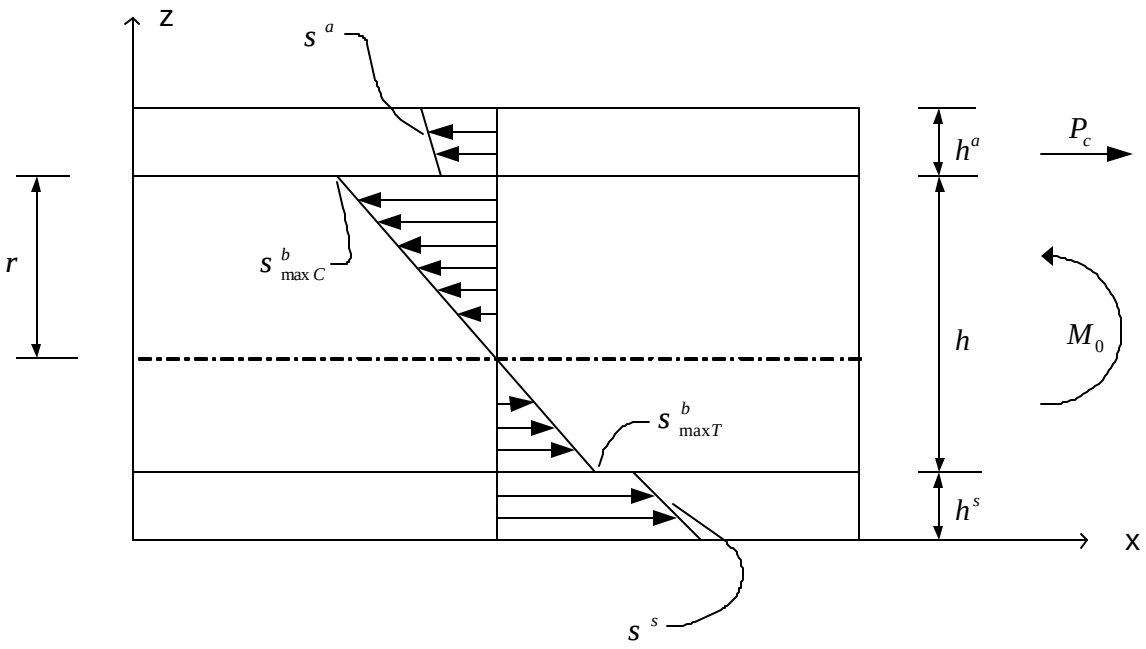

Figure 2.5 Beam Section

To obtain another equation the sum of moments around the neutral axis is calculated (figure 2.5). Since the sensor and actuator layer are small compared to the beam layer, it can again be assumed that the stresses in the actuator and sensor layer are constant, which leads to:

$$\begin{aligned}
&\sum M_{NA} = 0 \\
&\Rightarrow \int_A z \cdot s \; dA = -M_{eq} \\
&\Rightarrow \int_{A^a} z \cdot s \; dA + \int_{A^b} z \cdot s \; dA + \int_{A^s} z \cdot s \; dA = -M_{eq} \qquad (2.32) \\
&\Rightarrow -s_{11}^{a} \cdot h^a \cdot b \cdot \left(r + \frac{h^a}{2} \right) + \frac{2}{3} \cdot s_{\max C}^{b} \cdot r^2 \cdot b + \frac{2}{3} \cdot s_{\max T}^{b} \cdot b \cdot (h - r)^2 \\
&\qquad + s_{11}^{s} \cdot h^s \cdot b \cdot \left(h - r + \frac{h^s}{2} \right) = -M_{eq}
\end{aligned}$$

where M_{eq} is an equivalent moment that can be calculated through:

$$M_{eq} = M_0 - P_c \cdot \left(r + \frac{h^a}{2} \right) \qquad (2.33)$$

Now eight equations are available for the unknowns s_{11}^{a}, s_{11}^{s}, e_{11}^{a}, e_{11}^{s}, E_2^a, E_2^s, q_2^a, $s_{\max C}^{b}$, $s_{\max T}^{b}$, P_c, M_{eq}, r. Thus, more equations are needed to solve this system of equations. From figure 2.5 and similar triangle relations, the following can be derived:

$$\frac{s_{\max C}^{b}}{r} = \frac{s_{\max T}^{b}}{h - r} \qquad (2.34)$$

Euler-Bernoulli Beam theory states furthermore that plane sections remain plane, which leads to:

$$\frac{e_{11}^{a}}{r + h^a} = \frac{e_{11}^{s}}{h - r + \frac{h^s}{2}} \qquad (2.35)$$

Figure 2.6 shows a simplified deformed beam. Using this figure a strain relationship can be derived. The maximum tension stress in the base beam occurs at the lower side of the base beam and can be described as:

$$s^{b}_{\max T} = e^{b}_{\max T} \cdot D^{b} \tag{2.36}$$

The arc length in general is defined as:

$$L = r \cdot q \tag{2.37}$$

and can be used to calculate the strain at the low side of the base beam by using the strain definition:

$$e = \frac{\Delta L}{L} \tag{2.38}$$

the strain becomes to:

$$e^{b}_{\max T} = \frac{\Delta L}{L} = \frac{(r + h - r) \cdot q - r \cdot q}{r \cdot q} = \frac{h - r}{r} \tag{2.39}$$

Now equation 2.39 can be inserted into equation 2.36 and solved for r:

$$r = \frac{D^{b} \cdot (h - r)}{s^{b}_{\max T}} \tag{2.40}$$

Similar, a formulation for the strain in the sensor can be derived to:

$$e^{s}_{11} = \frac{h - r + \frac{h^{a}}{2}}{r} \tag{2.41}$$

and equation 2.40 can be inserted into equation 2.41, leading to:

$$e^{s}_{11} = s^{b}_{\max T} \cdot \frac{h - r + \frac{h^{a}}{2}}{D^{b} \cdot (h - r)} \tag{2.42}$$

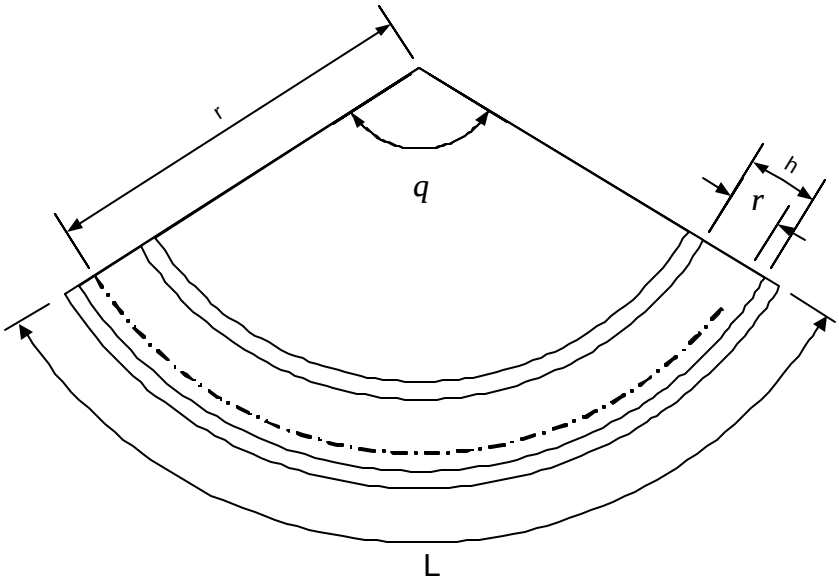

Figure 2.6 Deformed Beam

The last equation needed to solve this system of equations defines a relationship for the control force in the piezoelectric actuator. Two effects produce the electric field in the actuator: induced strain due to deformation of the beam and the applied control. The electric field due to the induced strain can be calculated using the second equation of the piezoelectric constitutive equations and setting the electric surface charge density of the actuator (q_2^a) equal to zero:

$$0 = e_{211}^a \cdot e_{11}^a + p_{22}^a \cdot E_2^a \tag{2.43}$$

This allows solving for the electric field induced by the strain:

$$E_{2\ ind}^a = -\frac{e_{211}^a \cdot e_{11}^a}{p_{22}^a} \tag{2.44}$$

The electric field of the actuator produces a stress in the actuator that results in the control force. The induced electric field needs to be subtracted, which leads to:

$$\begin{aligned} P_c &= A^a \cdot e_{211}^a \cdot \left(E_2^a - E_{2\ ind}^a\right) \\ &= A^a \cdot e_{211}^a \cdot \left(E_2^a + \frac{e_{211}^a \cdot e_{11}^a}{p_{22}^a}\right) \end{aligned} \tag{2.45}$$

Equations 2.22, 2.23, 2.24, 2.25, 2.30, 2.31, 2.32, 2.33, 2.34, 2.35, 2.42 and 2.45 are used to solve for all unknowns by using the commercial software MAPLE. The calculated equivalent moment can than be inserted into the displacement equation, which is defined as:

$$d_{tip} = \frac{M_{eq} \cdot L^2}{2 \cdot \left(DI\right)_{eq}} \tag{2.46}$$

for the free end. $\left(DI\right)_{eq}$ be calculated through:

$$\left(DI\right)_{eq} = D_1^b \cdot I^b + D_1^a \cdot I^a + D_1^s \cdot I^s \tag{2.46}$$

Figure 2.7 shows the calculated displacement of the analytical solution and the displacement calculated by FEM for different gains. It is visible that the FEM solution shows less displacement for lower gains than the analytic solution. This can be explained by two reasons. The first reason is that different assumptions have been made for the calculations. The analytic solution was calculated by using the Euler-Bernoulli Beam Theory, whereas the FEM calculation used the elasticity theory. The elasticity theory takes Poisson's ratio into account and is about 10% stiffer compared to the Euler-Bernoulli Beam Theory. This trend is in compliance with the solutions shown here. However, the difference between the analytic solution and the FEM result is about 17% to 24% and is therefore higher then it is supposed to be. This can be explained with the fact that the FE solution has not converged completely. The geometry has been modeled with 250 elements in each layer, which results in an aspect ratio of ten to one for the piezoelectric elements. A representation of the geometry with more elements would result in a less stiff structure and the displacement would therefore be closer to the analytic solution. A calculation using more elements has not been conducted, as building a new finite element model is a very time consuming process, in which a completely new input-file has to be written. Since a calculation for a gain of zero needs no implementation of the control law, a finite element calculation using more elements can be done quickly. The solution using piezoelectric elements with an aspect ratio of one to five is shown as a point at zero gain. One can see that this result is much closer to the analytic solution. The difference is about 7%, which shows an excellent compliance with difference in the different theories. It is furthermore visible, that the slopes of both calculations are almost identical. This is expected and verifies the finite element calculation.

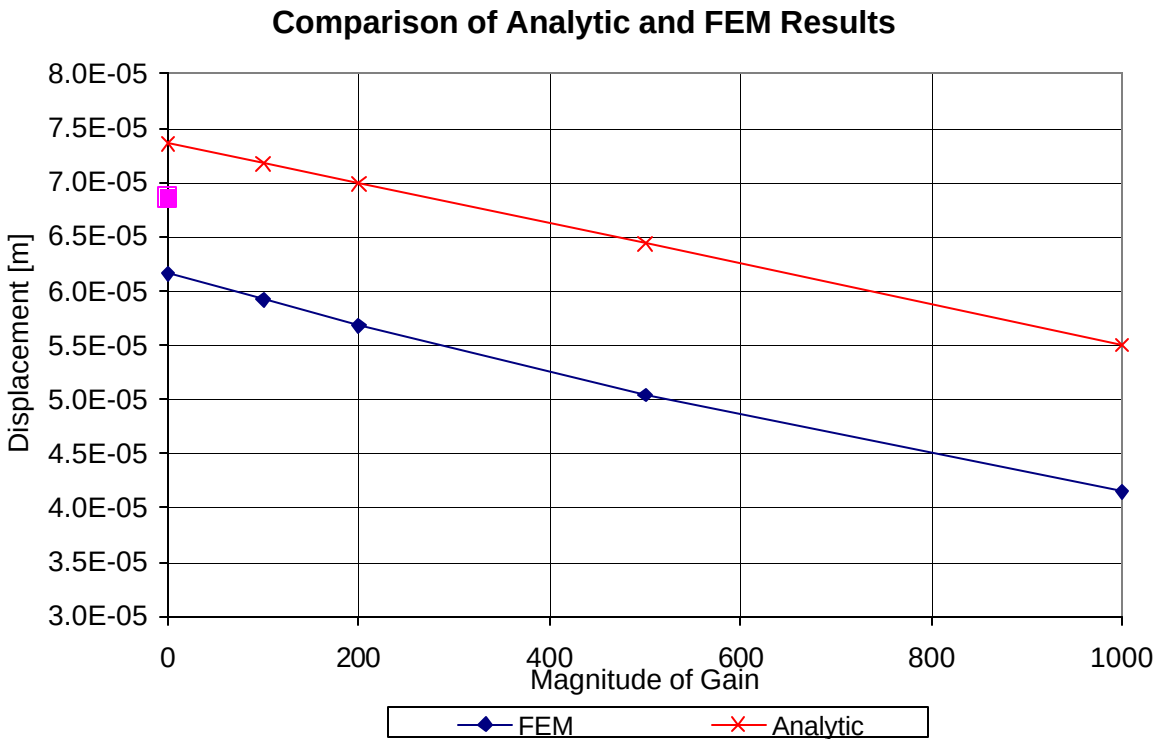

Figure 2.7 Comparison of tip displacement of the Tzou-Beam for different Gains

Figure 2.8 shows the relative difference between the displacement for a gain of zero and other gains. It is visible that the relative difference of the displacement is very small for lower gains. The relative difference of displacement between the displacement of gain 0 and gain 500 is about 18% for the FEM solution and about 13% for the analytic solution. This shows a good compliance of the analytic and the FEM solution. Even at gain of 1000 the relative displacement of the FEM calculation is about 33% compared to 25% for the analytic solution. This is a difference of 12%, which is acceptable considering that different assumptions have been made for both calculations.

For these reasons it is to say, proper implementation for the static case is validated.

2.3 DYNAMIC CALCULATION – PROPORTIONAL CONTROL

The finite element equations for modeling a linear piezoelectric material were developed by Naillon *et al.* (1983) and Lerch (1990). Considering time harmonic excitation, these equations may be written as:

$$\left(-w^2\begin{bmatrix} M & 0 \\ 0 & 0 \end{bmatrix}+\begin{bmatrix} K_{uu} & K_{u\Phi} \\ K_{\Phi u} & -K_{\Phi\Phi} \end{bmatrix}\right)\begin{Bmatrix} U \\ \Phi \end{Bmatrix}=\begin{Bmatrix} F \\ Q \end{Bmatrix} \tag{2.47}$$

This system of equations describes the finite element model for piezoelectric materials without considering damping effects. This assumption is appropriate for this study, since the piezoelectric sensor and actuator layer are very thin compared to the base structure. Therefore, the piezoelectric material has almost no influence on the damping characteristic. The implementation of proportional control is basically the same as in the static case. The control law is formulated as:

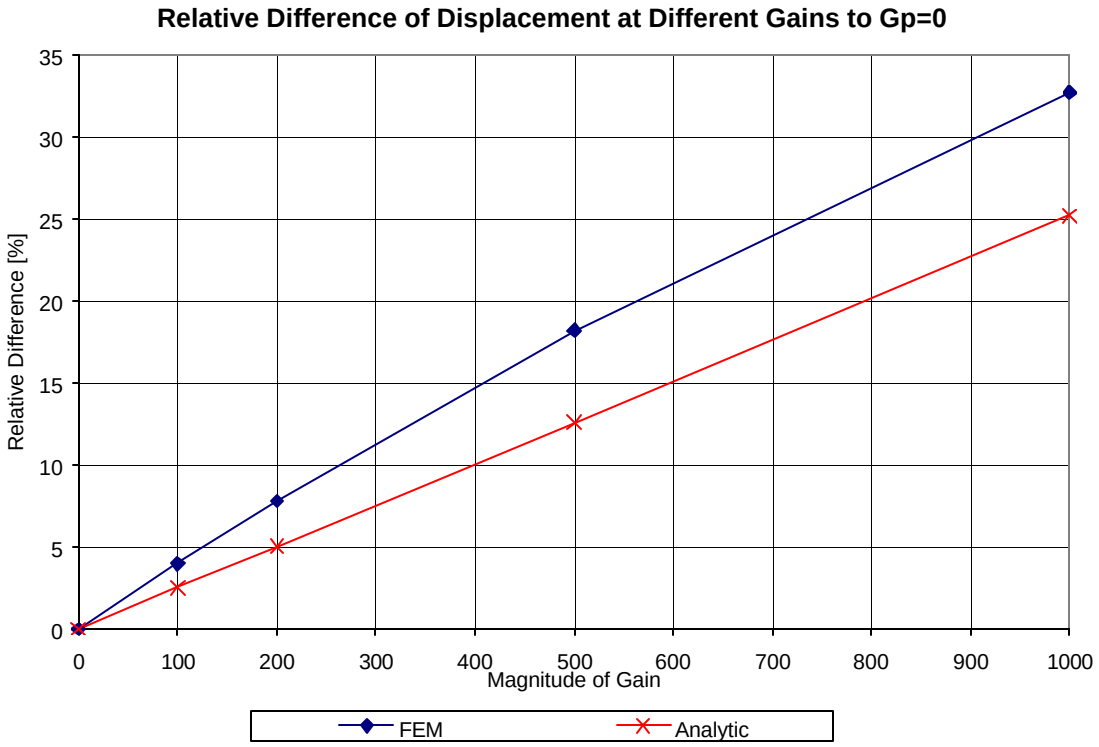

Figure 2.8 Relative Differences

$$\{\Phi^a\} = [G_p] \cdot \{\Phi^s\} \tag{2.48}$$

and inserted into the stiffness matrix exactly as in the static case. Since the mass matrices have no influence on the control, the mass matrices remain unchanged. Therefore, the finite element formulation for a piezoelectric material including a proportional control loop can be written as:

$$\left(-w^2 \begin{bmatrix} M^s & 0 & 0 & 0 \\ 0 & 0 & 0 & 0 \\ 0 & 0 & M^a & 0 \\ 0 & 0 & 0 & 0 \end{bmatrix} + \begin{bmatrix} K^s_{uu} & 0 & K^s_{u\Phi} & 0 \\ K^s_{uu} & 0 & K^s_{\Phi\Phi} & 0 \\ 0 & K^a_{uu} & K^a_{u\Phi} \cdot G_p & 0 \\ 0 & K^a_{\Phi u} & K^a_{\Phi\Phi} \cdot G_p & 0 \end{bmatrix} \right) \begin{Bmatrix} U^s \\ \Phi^s \\ U^a \\ \Phi^a \end{Bmatrix} = \begin{Bmatrix} F^s \\ Q^s \\ F^a \\ Q^a \end{Bmatrix} \tag{2.49}$$

where M^s and M^a represent the sensor and actuator mass matrices, respectively.
As described in the static case proportional control can be implemented in two ways, first by applying a node-to-mode control or second by applying a layer-to-layer control. For the layer-to-layer control the same method is used as in the static case.

2.3.1 IMPLEMENTATION OF PROPORTIONAL CONTROL

The implementation of the control law into the finite element code ABAQUS is done through an identical process as in the static case. For dynamic calculations it is necessary to include the mass matrices in the calculation. Since the mass matrices have no influence on the control they are written out by ABAQUS and read back in without any modification.

ABAQUS is not able to read in a stiffness matrix for big models with a great number of elements, as ABAQUS requires a large amount of memory for this process. Even increasing the memory works only up to a limit of 2 GB since ABAQUS is limited

in the SOLARIS 8 system to this amount of memory. Since it is necessary for layer-to-layer control to read in the complete stiffness matrix another approach has been taken by assembling the complete stiffness and mass matrix in MATLB and solving the system in MATLAB.

2.3.2 VERIFICATION OF PROPORTIONAL CONTROL

In the first step of the verification of the implementation of proportional control the system shown in figure 2.3 is used again. In this case the system is excited through a steady-state harmonic excitation, instead of a static load. Since the analytic solution to this problem is not trivial the results will be compared at low frequencies only, as the system is stiffness dominated for low frequencies and mass or damping dominated near its natural frequency. This should be sufficient for verifying the technique outlined above, as the mass matrices are not modified. For low frequencies the difference between the actuator and sensor displacements must be very close to the static case, since a frequency of zero corresponds to the static case. The difference between sensor and actuator displacement from the static case can be obtained from table 2.2 by:

$$d_s = u^a - u^s = 1.2073 \cdot 10^{-5} - 4.9497 \cdot 10^{-6} = 7.1233 \cdot 10^{-6} \tag{2.50}$$

where the superscript “s” indicates the static case. Table 2.4 compares the result for a system modeled with 10 elements for the actuator and sensor, respectively, for different frequencies and a proportional gain of 240. It is visible that the error increases with increasing frequency. However, this does not indicate an actual error in the calculation. It is more that the mass which was neglected for the theoretical comparison, becomes more

Table 2.4 Validation for proportional control (decoupled system)

Frequency	Displacement [m]		Difference in Displacement [m]	Error (%) against the static case
	Sensor	Actuator		
Static	4.94970E-06	1.20730E-05	7.12330E-06	--
10.0	4.94975E-06	1.20735E-05	7.12375E-06	0.01
90.6	4.95449E-06	1.20968E-05	7.14231E-06	0.26
211.5	4.97595E-06	1.22024E-05	7.22645E-06	1.18
292.1	5.00007E-06	1.23218E-05	7.32173E-06	1.32
413.0	5.05163E-06	1.25794E-05	7.52777E-06	2.81

dominant. Figure 2.9 shows the frequency diagram for a proportional gain of 240. It shows furthermore a verification calculation, which was done in ABAQUS just for the sensor to confirm that the sensor has the frequency-diagram remains the same after implementation of the control. It is visible, that the resonant frequency of the actuator and sensor are identical. It is furthermore visible, that the displacement of the sensor in the new model is identical to the verification calculation. This indicates a good accordance with the theory.

In the second step, the sensor and actuator elements are coupled over a base beam structure. The modeled system is taken again from Tzou (1993) and shown in figure 2.4. The properties of the model are shown in table 2.5. A damping ratio of 0.02 was assumed in the base beam (as in Tzou, 1993). This was implemented in ABAQUS using Rayleigh damping, as this can be easily implemented within ABAQUS. For this study, the beam has been modeled with 250 elements along each layer. This assures an aspect ratio smaller then one to ten for all elements, which is appropriate for linear elements that have been used to model this system. The results of the finite element calculation are compared with the results published by Tzou and are shown in table 2.6. It is visible that the natural frequency calculated by the FEM computation without applied control (Gp=0) is higher than calculated by Tzou. This can be explained with the fact, that the FEM modeled is stiffer than the actual system, since an aspect ratio of one to ten is the upper limit for linear elements. The resonant frequency of the FEM calculation would decrease with more elements. It is furthermore visible that the proportional gain in the Tzou calculation has almost no influence on the resonant frequency. This is different in the FEM calculation. The resonant frequency decreases dramatically with higher gains. This

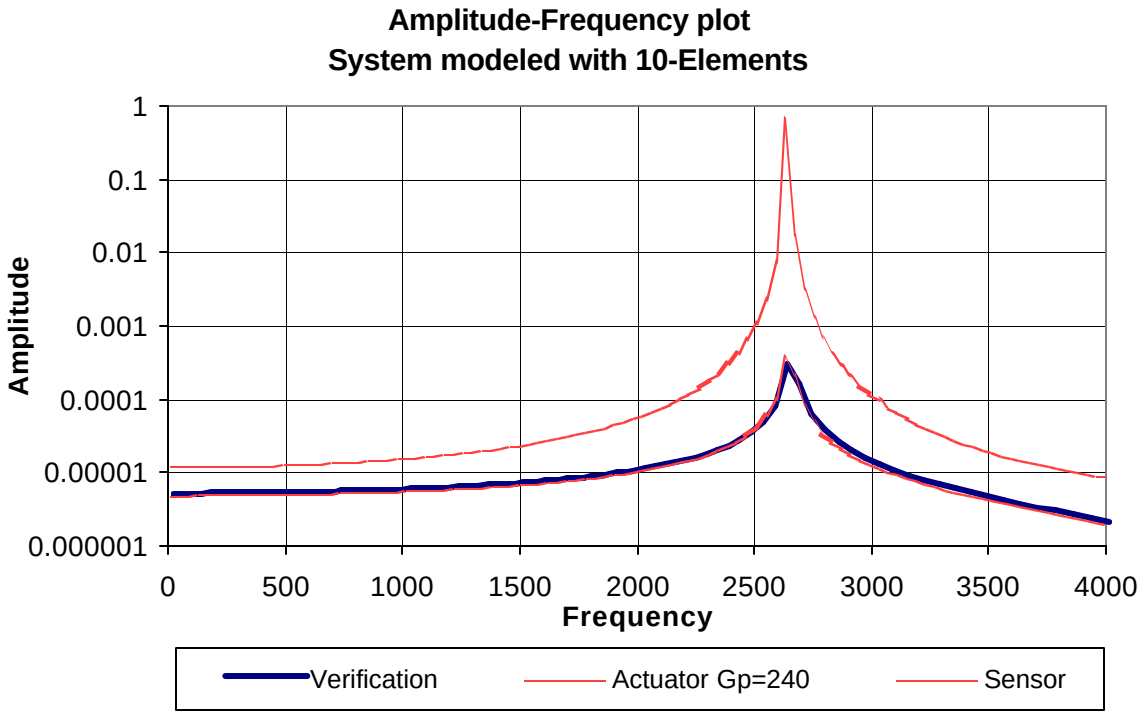

Figure 2.9 Frequency-diagram for proportional control (decoupled system)

Table 2.5 Properties of the Tzou beam (dynamic)

Plexiglas Beam	
Young's Modulus	$D = 3.1028 \cdot 10^{9} \frac{N}{m^2}$
Mass Density	$r = 1190.0 \frac{kg}{m^3}$
Thickness	$h = 1.6 \cdot 10^{-3}\, m$
Width	$b = 0.01m$
Length	$L = 0.1m$
Poisson's ratio	$m = 0.3$
Rayleigh damping factors	$a = 0,\ b \approx 1.35 \cdot 10^{-4}$
Sensor/Actuator Layer	
Young's Modulus	$D^s = D^a = 2.00 \cdot 10^{9} \frac{N}{m^2}$
Mass Density	$r^a = r^s = 1800.0 \frac{kg}{m^3}$
Sensor/Actuator thickness	$h^a = h^s = 40\,mm$
Dielectric constant	$p^a = p^s = 1.06481 \cdot 10^{-10} \frac{F}{m}$
Piezoelectric constant	$e_{311}^a = e_{311}^s = 0.046 \frac{V\,m}{N}$

Table 2.6 Comparison Tzou vs. FE results of proportional control calculations

Proportional Feedback Gain	Natural Frequency First Mode [Hz]			Loss Factor		
	Tzou	FEM Calculation	Error (%)	Tzou	FEM Calculation	Error (%)
0	41.735	44.56	6.77	0.04	0.039	-2.50
100	41.67	43.6	4.63	0.040062	0.039725	-0.84
500	41.38	40.08	-3.14	0.040344	0.042778	6.03
1000	41.072	35.7	-13.08	0.040646	0.046339	14.01

influences the loss factor as well, since it is calculated by the half power bandwidth method. According to this method, the loss factor is defined as:

$$h = \frac{w_2 - w_1}{w_n} \tag{2.51}$$

where w_n describes the natural frequency. w_1 and w_2 can be found by calculating:

$$A_{HB} = \frac{A_n}{\sqrt{2}} \tag{2.52}$$

and finding the corresponding frequencies to these amplitudes. Figure 2.10 shows the amplitude-frequency diagram for proportional gains of 0, 100, 500 and 1000, respectively. Since no additional damping is added to the system by applying proportional feedback control, the change in the loss factor is only due to the change in natural frequency. The results of this calculation differ from a simple one-dimensional spring-mass-damping system, where the loss factor is independent of the resonant frequency.

The same calculations have been done with proportional layer-to-layer control. Since the calculation had to be done completely in MATLAB, fewer points have been chosen to plot the amplitude-frequency diagram, since MATLAB requires high computational power to solve big matrix equations. For this reason, a comparison of the loss factors is not meaningful, since it is not possible to calculate an accurate loss factor without enough resolution. A comparison of the natural frequencies is shown in table 2.7. It is visible, that the natural frequency does not decrease as fast using layer-to-layer control as by using node-to-node control. However, the difference of the natural frequency at a proportional gain of 100 between the Tzou solution and the FEM solution

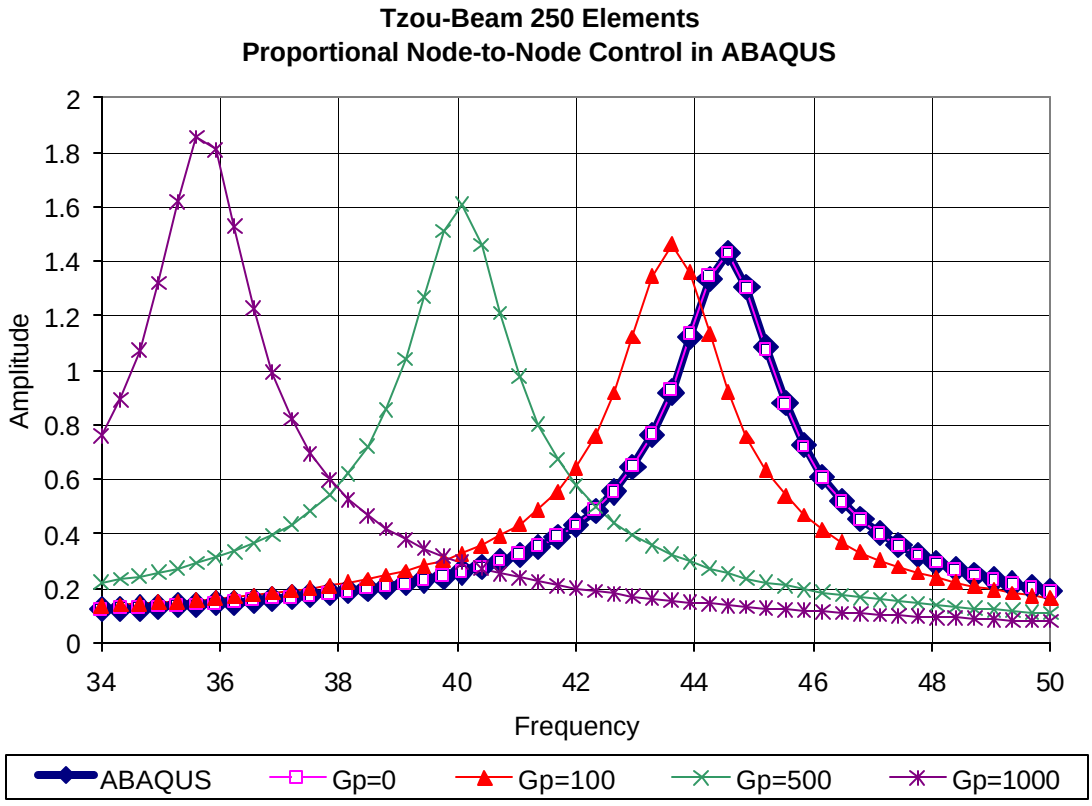

Figure 2.10 Frequency diagram of Tzou beam (finite element calculation)

Table 2.7 Comparison of the natural frequency of the Tzou beam (proportional control)

Proportional Feedback Gain	Tzou	Node-to-Node			Layer-to-Layer		
		Frequency	Error (%)	Comp. Time (hours)	Frequency	Error (%)	Comp. Time (hours)
0	41.735	44.56	6.77	3.2	44.67	7.03	24.1
100	41.67	43.6	4.63	3.2	44.00	5.59	24.1
500	41.38	40.08	-3.14	3.2	41.50	0.29	24.1
1000	41.072	35.7	-13.08	3.2	38.50	-6.26	24.1

is too large. For easier visualization figure 2.11, shows the frequency-amplitude diagram for a proportional gain of 1000 for node-to-node and layer-to-layer control.

We were unable to obtain satisfactory results for the dynamic calculation using proportional control, since published results could not be repeated.

2.4 DYNAMIC CALCULATION - DERIVATIVE CONTROL

Tzou (1993) shows, that proportional control is not well suited for use in active damping structures. Proportional control only has influence on the natural frequency, but leaves the damping ratio nearly unchanged. Since the goal of active damping is to increases the damping effectiveness, proportional is not a good choice. For this reason, derivative control has also been implemented for dynamic calculations.

2.4.1 IMPLEMENTATION OF DERIVATIVE CONTROL

The feedback signal from the actuator to the sensor is now represented as:

$$\{\underline{\Phi}^a\} = [G_d] \cdot \{\dot{\underline{\Phi}}^s\} \tag{2.53}$$

where $[G_d]$ represents the derivative control gain matrix and the underscore indicates that the variable is time dependent. For a harmonic excitation the sensor potential can be written as:

$$\{\underline{\Phi}^s\} = \{\Phi^s\} e^{iwt} \tag{2.54}$$

and the according derivative as:

$$\{\dot{\underline{\Phi}}^s\} = iw\{\Phi^s\} e^{iwt} \tag{2.55}$$

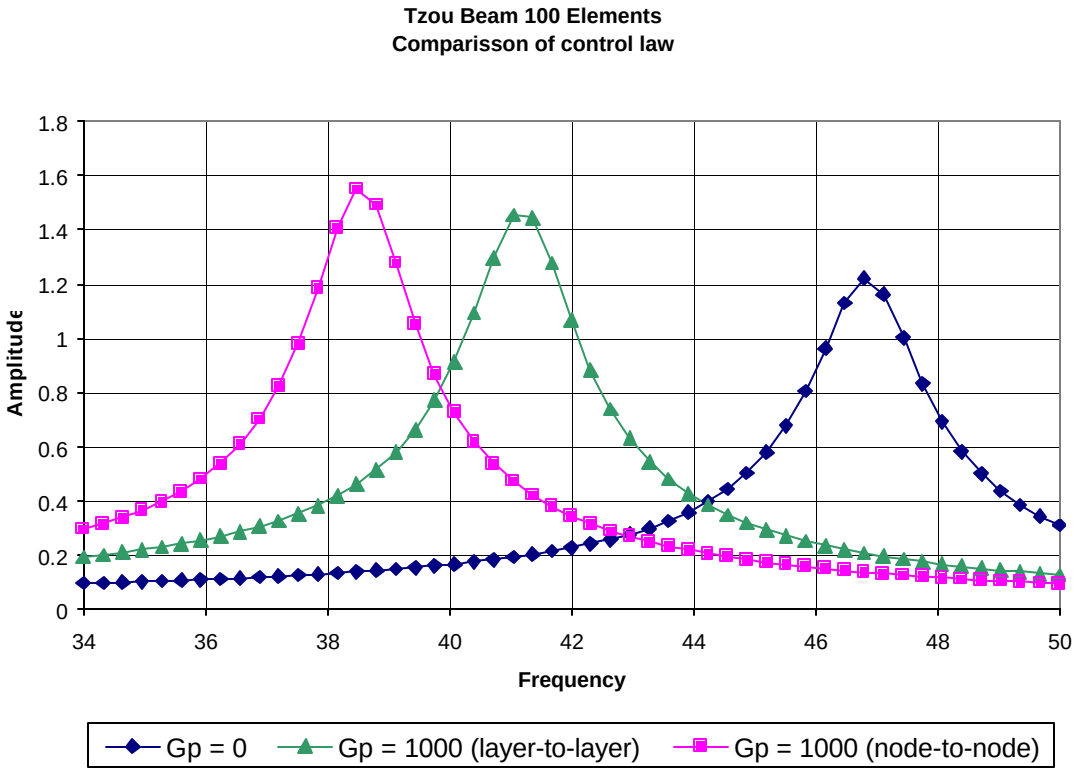

Figure 2.11 Frequency diagram of the Tzou beam (proportional control)

Now, equation 2.55 can be inserted into equation 2.53, which leads to:

$$\left\{\underline{\Phi}^{a}\right\} = iw\left[G_d\right]\left\{\Phi^{s}\right\}e^{iwt} \tag{2.56}$$

For Node-to-Node control the gain matrix can be simplified to:

$$\left[G_d\right] = G_d\left[I\right] \tag{2.57}$$

where $\left[I\right]$ is the identity matrix.

Since the matrix terms associated with $\underline{\Phi}^{a}$ are now ninety degrees out of phase, a new damping matrix must be included in equation 2.49. The complete finite element formulation for a piezoelectric material with a derivative feedback gain can be written as:

$$\left(-w^2\begin{bmatrix} M^s & 0 & 0 & 0 \\ 0 & 0 & 0 & 0 \\ 0 & 0 & M^a & 0 \\ 0 & 0 & 0 & 0 \end{bmatrix} + iw\begin{bmatrix} 0 & 0 & 0 & 0 \\ 0 & 0 & 0 & 0 \\ 0 & 0 & K^a_{u\Phi}\cdot G_d & 0 \\ 0 & 0 & K^a_{\Phi\Phi}\cdot G_d & 0 \end{bmatrix} + \begin{bmatrix} K^s_{uu} & 0 & K^s_{u\Phi} & 0 \\ K^s_{uu} & 0 & K^s_{\Phi\Phi} & 0 \\ 0 & K^a_{uu} & 0 & K^a_{u\Phi} \\ 0 & K^a_{\Phi u} & 0 & K^a_{\Phi\Phi} \end{bmatrix}\right)\begin{Bmatrix} U^s \\ \Phi^s \\ U^a \\ \Phi^a \end{Bmatrix} = \begin{Bmatrix} F^s \\ Q^s \\ F^a \\ Q^a \end{Bmatrix} \tag{2.58}$$

where the middle matrix describes the damping matrix of the piezoelectric material.

To implement layer-to-layer control equation 2.9 must be change to:

$$\begin{Bmatrix} \underline{\Phi}^a_1 \\ \underline{\Phi}^a_2 \\ \underline{\Phi}^a_3 \\ \vdots \\ \underline{\Phi}^a_n \end{Bmatrix} = \frac{G_p}{n}\begin{bmatrix} 1 & 1 & 1 & 1 & 1 & 1 & \cdots & 1 \\ 1 & 1 & 1 & 1 & 1 & 1 & \cdots & 1 \\ 1 & 1 & 1 & 1 & 1 & 1 & \cdots & 1 \\ \vdots & \vdots & \vdots & \vdots & \vdots & \vdots & \ddots & \vdots \\ 1 & 1 & 1 & 1 & 1 & 1 & \cdots & 1 \end{bmatrix}\begin{Bmatrix} \underline{\dot{\Phi}}^s_1 \\ \underline{\dot{\Phi}}^s_2 \\ \underline{\dot{\Phi}}^s_3 \\ \vdots \\ \underline{\dot{\Phi}}^s_n \end{Bmatrix} \tag{2.59}$$

and the averaged values can be insert into the damping matrix in equation 2.58.

ABAQUS has no way of defining the damping matrix directly. The easiest method in ABAQUS to include damping is Rayleigh damping, in which the damping matrix is defined as:

$$\left[C\right] = a\left[M\right] + b\left[K\right] \tag{2.60}$$

where $[M]$ and $[K]$ are the mass and stiffness matrix and a and b the Rayleigh damping coefficients, respectively. Since the finite element code ABAQUS offers no possibility to define a damping matrix directly, a novel approach had to be developed in order to create a stiffness matrix as derived in equation 2.58. This approach can be summarized in three steps:

1. An additional element is created with a stiffness $[K^*]$
2. The damping matrix is defined in terms of this matrix

$$[C] = b[K^*] \tag{2.61}$$

where $b = 1$

3. A third element is created $[K^{**}]$ with the property:

$$[K^{**}] = -[K^*] \tag{2.62}$$

to substract out the stiffness of $[K^*]$, as it is not part of the stiffness of the actual system.

2.4.2 VERIFICATION OF DERIVATIVE CONTROL

To verify the correct implementation of the derivative control a two-step approach is used again. In the first step the mechanical system shown in figure 2.3 is used and excited harmonically. As was done for proportional control, the analytic solution to this system is not trivial and therefore the mass influence is neglected for the verification. For this reason, the theoretical values are compared with the finite element calculations at low frequencies only, since the system is stiffness dominated for low frequencies.

The constitutive law for the one-dimensional case from equations 2.1 and 2.2 is valid as well for the static case as for the dynamic case. For harmonic excitations, the stress is a function of time and can be written as:

$$s_{11}^{s} = \frac{F}{A} \cdot e^{iwt} \tag{2.63}$$

The control law described in equation 2.53 to 2.56 can now be simplified to:

$$\underline{E}_2^a = G_d \cdot \underline{\dot{E}}_2^s \tag{2.64}$$

where the underscore indicates that the variable is time dependent. The electric field of the sensor for harmonic excitations can also be written as:

$$\underline{E}_2^s = E_2^s \cdot e^{iwt} \tag{2.65}$$

and accordingly the time derivative of the electric field:

$$\underline{\dot{E}}_2^s = i \cdot w \cdot E_2^s e^{iwt} \tag{2.66}$$

which is inserted into equation 2.64 and becomes:

$$\underline{E}_2^a = i \cdot w \cdot G_d \cdot E_2^s \cdot e^{iwt} \tag{2.67}$$

With this relationship and the constitutive equations it is now possible to calculate the strain of the actuator as:

$$\underline{e}_{11}^a = i \frac{e_{211}^a \cdot G_d \cdot w \cdot E_2^s}{D_1^a} e^{iwt} \tag{2.68}$$

where the middle part of equation 2.68 describes the amplitude, which is compared in this verification.

Table 2.8 shows the theoretical values and the results of a finite element calculation for the decoupled mechanical system shown in figure 2.3. It is visible that the

Table 2.8 Validation for derivative control (decoupled system)

Frequency	Displacement [m]		Difference [m]	Error (%)
	Theory	FEM Calculation		
1	1.58039E-05	1.58039E-05	0	0.00
90.97	0.001440839	0.001437677	-3.16208E-06	-0.22
210.93	0.003373241	0.003333509	-3.97323E-05	-1.18
300.9	0.004871907	0.004755382	-0.000116525	-2.39
390.87	0.006436248	0.006177256	-0.000258992	-4.02

error for low frequencies is negligible. However, by approaching the natural frequency the mass becomes dominant for the solution and the theoretical values shown here are no longer accurate.

In the second step the sensor and actuator layers are coupled by a base beam again. The same system has been used, which was used for the verification of the proportional control and is shown in figure 2.4 with the according properties in table 2.5. The results of the FEM calculation are compared again against the solution published by Tzou (1993). The results of this comparison are shown in table 2.9. It is visible, that the derivative gain used by Tzou is much higher then the derivative gain used in the FEM calculation. Gains in the order of magnitude used by Tzou result in over damped solutions for the FEM calculation. To achieve results with reasonable loss factors the gain was reduced. Tzou shows furthermore, that a derivative gain of 100 is almost an optimal value for damping of the first mode, bigger values are less effective and the loss factor is decreasing. Tzou explains this effect with the fact, that higher gains change the boundary condition at the free end to a sliding-roller boundary condition. This effect can only be observed if a layer-to-layer control is applied, since a node-to-node control has almost no effect at the free end. It was not tried to implement layer-to-layer control for derivative control, since the implementation of layer-to-layer control for proportional control resulted in extremely long computation times.

The FEM calculation shows that increasing derivative gain increases the loss factor and is therefore contrary to the Tzou results. It is also observed, that increasing gain in the Tzou results increases the first natural frequency. This could not be repeated by the FEM calculation, which shows an identical natural frequency for all derivative

Table 2.9 Comparison Tzou vs. FE results of derivative control calculation

Tzou			FEM		
Derivative Feedback Gain	Natural Frequency First Mode [Hz]	Loss Factor	Derivative Feedback Gain	Natural Frequency First Mode [Hz]	Loss Factor
0	41.7	0.000	0	44.56	0.000
100	54.79	0.331	0.5	44.56	0.058
500	66.06	0.070	1	44.56	0.116
1000	66.24	0.036	2	44.56	0.233

gains. For clarification, the frequency response shows for the FEM calculation of the Tzou beam for different derivative gains is shown in Figure 2.12.

In conclusion, I was not able to obtain satisfactory results for the implementation of proportional and derivative gain. The results of the static calculation are the only validated results and are therefore used for the study.

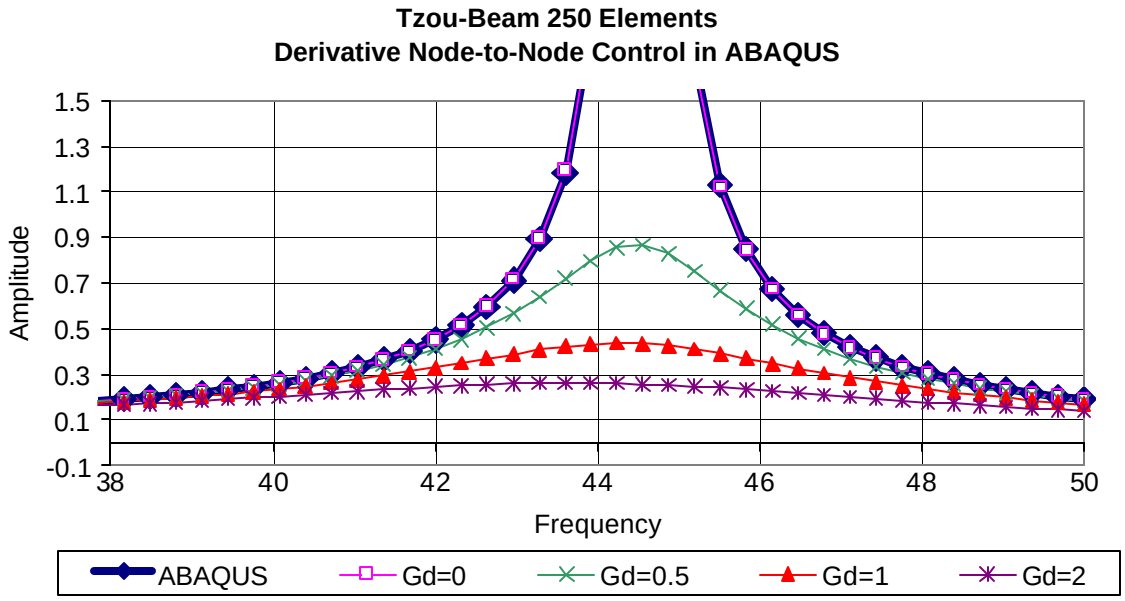

Figure 2.12 Frequency diagram of the Tzou beam (derivative control)

3 OPTIMIZATION

The concept of optimization is a basic idea in engineering. The desire to improve design, for example, to make products better, lighter, cheaper or more reliable, has been a major idea since early engineering years. Numerical optimization has been proven to be a useful tool for improving complex designs. This chapter gives an overview of the general idea of optimization routines used and how the optimization problem is set up for the given case.

3.1 INTRODUCTION

In general, an optimization problem begins with a set of independent design variables and usually includes conditions or restrictions that define acceptable values for these variables. For given values of design variables it must be possible to compute an objective function, which gives a measure for the "goodness" of the design. In mathematical terms, optimization is the minimization or maximization of an objective function within given constraints on the design variables. The general form of an optimization problem can be expressed in mathematical terms as:

$$\min_{x \in R^n} F(\vec{x})$$

$$\text{subject to} \quad h_i(\vec{x}) = 0, \quad i = 1, 2, ..., m \tag{2.1}$$

$$g_i(\vec{x}) \leq 0, \quad i = 1, 2, ..., l$$

where it is assumed, that the objective and constraint functions are continuous real-valued scalar functions.

3.2 GENERAL TOPOLOGY OPTIMIZATION

The traditional way of finding the best shape or topology for a mechanical structure is an iterative trail-and-error approach. The design engineer uses his experience and intuition to find a solution to a given problem. Mechanical or numerical tests then show if the design meets the specified criteria. If the design fails, the design engineer enhances the design until a satisfying result is found. This system requires both special skill and experience for a truly good design and it does not guarantee that the best possible design has been found.

Structural shape optimization can be thought of as determination of the optimal spatial material distribution. In other words, for a given set of loads and boundary conditions, the material is redistributed in order to minimize the objective. Therefore, the general shape optimization problem can be considered as a point-wise material/no-material approach. However, implementation of this on-off approach to an optimization problem requires the use of discrete optimization algorithms. Such approaches have been shown to be time consuming and unstable, unless composite materials are introduced (Hassani and Hinton 1999). Considering a composite consisting of an infinite number of small holes, which are periodically distributed, can solve this problem (figure 3.1). In fact, using a cellular body with a periodic microstructure moves the on-off approach of the problem from the macroscopic scale to the microscopic scale (Bendsoe 1989). One approach to introduce these microstructures is homogenization. The theory of homogenization is used to determine the macroscopic mechanical properties of these materials. In practice, after choosing the design domain and the finite element discretization, it is assumed that each element consists of a cellular material with a specific microstructure. The geometrical

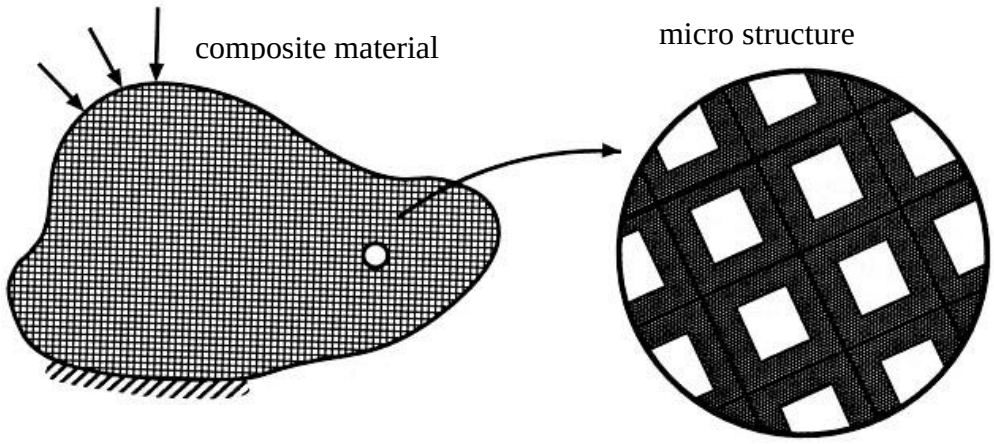

Figure 3.1 Homogenization through microcells with rectangular holes (Hassani and Hinton 1999)

parameters of these microstructures are the design variables of the optimization problem. In the simplest case the microstructure has rectangular holes or voids (as shown in figure 3.1) and the mechanical properties become proportional to the density of the material.

Figure 3.2 illustrates this process for the design of a bracket using homogenization, where the design domain and the boundary conditions are shown in Figure 3.2(a). The optimization process varies the density of each finite element, which is shown through a gray scale in the picture. A cell that is completely black corresponds to a density of 100%, where as a cell that is completely white corresponds to a density of 0%. The optimal material distribution for this problem (a stiff lightweight design) is shown in Figure 3.2(b). Since materials with intermediate densities are artificial and cannot be produced, this solution needs to be interpreted. This is done in Figure 3.2(c). Furthermore, general manufacturing rules can be applied, which leads to the final solution of this problem, shown in figure 3.2(d).

3.3 TOPOLOGY OPTIMIZATION IN THIS STUDY

Topology optimization using the homogenization method can be used for piezoelectric materials as shown by Silva *et al.* (1999). A homogenization approach using microcells with rectangular voids is used as described above, where the piezoelectric properties need to be considered additionally. The finite element formulation of piezoelectric materials has a stiffness tensor D_{ijkl}^{0}, a piezoelectric tensor e_{ijkl}^{0} and a dielectric tensor p_{ij}^{0} as described in chapter 2. If the basic material considered in the analysis is steel, the piezoelectric coefficients are zero, and the electric effect is not

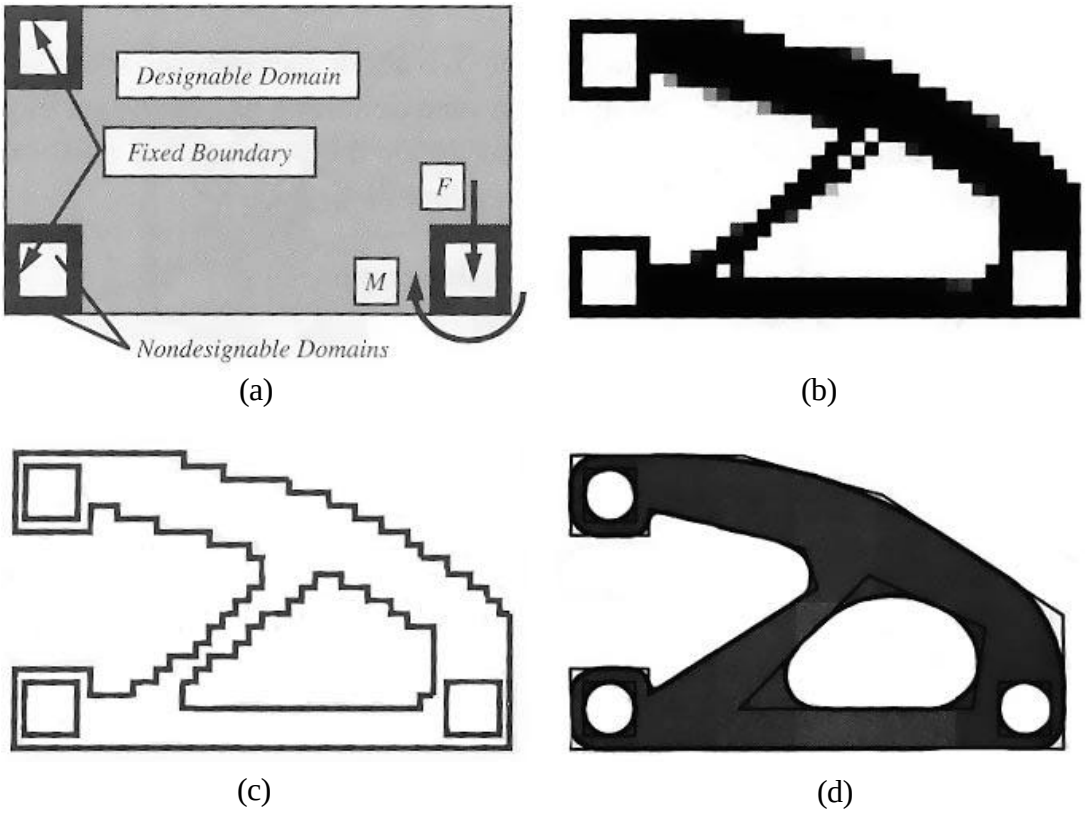

Figure 3.2 Optimal topology design (Papalambros and Douglas 2000)

considered. Therefore, the local tensor properties in each element *"n"* can be expressed in terms of one design variable x_n times the basic material property:

$$D_{ijkl}^{n} = x_n \cdot D_{ijkl}^{0} \qquad e_{ijkl}^{n} = x_n \cdot e_{ijkl}^{0} \qquad p_{ij}^{n} = x_n \cdot p_{ij}^{0} \tag{2.2}$$

where x_n represents the density of material in that element that ranges from x_{low} to 1. For $x_n = x_{low}$ the element is "void" and for $x_n = 1$ the element assumes the properties of the solid material. x_{low} has to be defined as a number greater than zero to avoid a singular stiffness matrix. For this study $x_{low} = 0.001$ has been used. Now the optimization problem can be formulated as:

$$\begin{aligned} &\text{minimize:} && u_{out} \\ &\text{subject to:} && 0 \le V_{ave} \le V_{ave}^{\max} \\ & && 0.001 \le x_n \le 1 \end{aligned} \tag{2.3}$$

where u_{out} is the displacement at the output point due to the force applied to the system, V_{ave} is the average volume in the design space and $V_{ave}^{\max}$ is the maximum allowed average volume in the design space. This constraint enables the possibility to define how much material shall be used to find the best solution.

For solving the above stated optimization problem, a sequential linear programming (SLP) algorithm is used. In SLP, the optimization problem is linearized around the current design point in each iteration and the next design is found by linear programming. The reason for using SLP is its robustness since the homogenization problem has numerous local minima and is not a well-behaved problem (Sigmund and Torquato 1997; Yi, Park et al. 2000). Before implementing the homogenization problem

into a commercial optimization code a software survey of seven different optimization programs has been conducted. The result of this survey led to choosing the VisualDOC as the program to be used in this study. For further details regarding the survey and the other examined optimization programs please refer to appendix A. For clarification a process diagram of the optimization process is shown in figure 3.3.

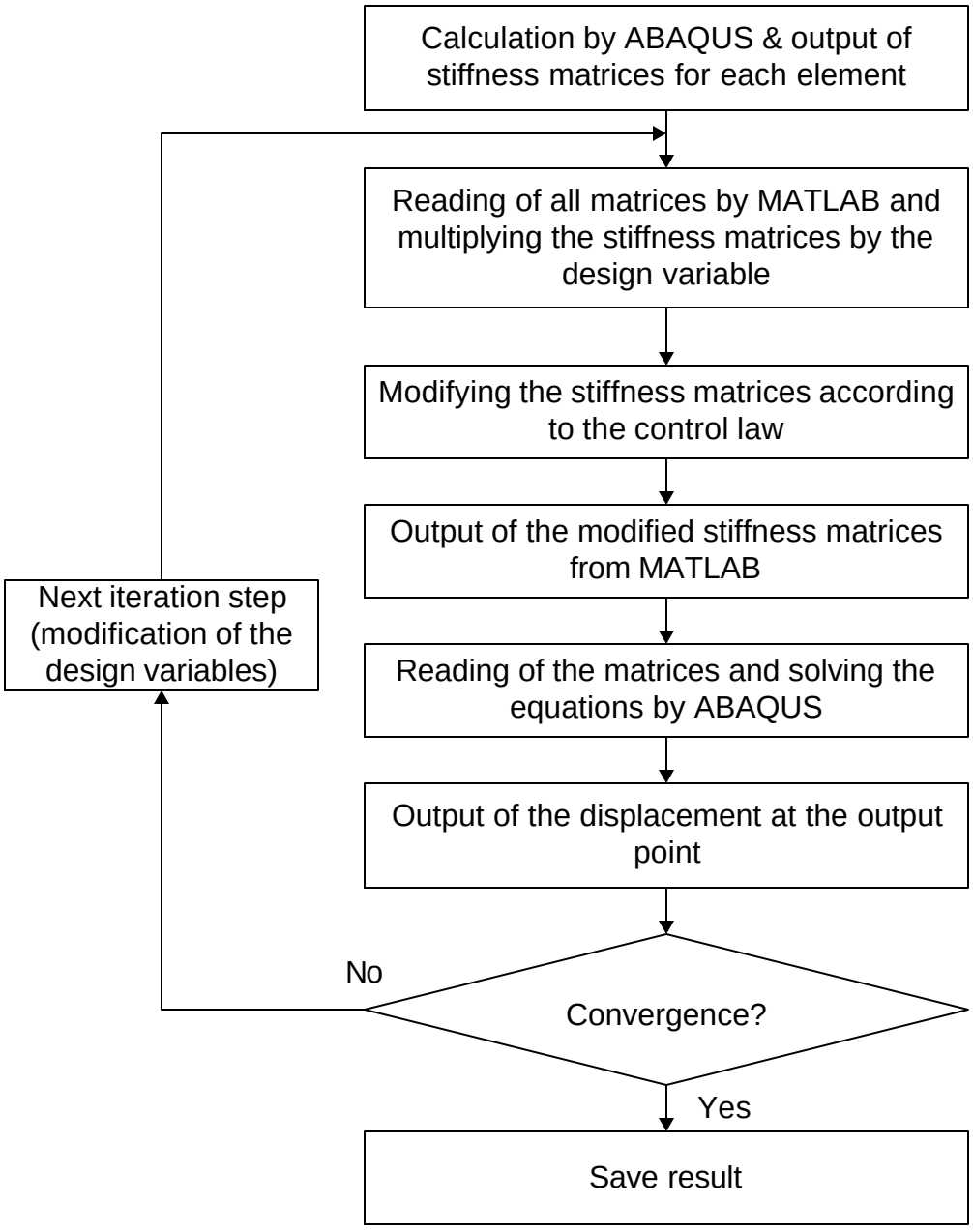

Figure 3.3 Optimization process diagram

4 RESULTS

A feedback control loop for static calculations using piezoelectric materials has been developed and implemented with the commercial finite element package ABAQUS. The goal is to determine the best topology of the piezoelectric actuator to minimize the tip deflection of a cantilever beam. This is a typical area of topology optimization. Since analytical solutions to this problem are not practical, the finite element calculation has been linked with a numerical optimization algorithm to determine the best topology.

This chapter shows the results of optimizations for two parameter studies, one with different feedback gains and another one with different amount of material used for the actuator. Both parameter studies have, furthermore, been conducted using two different thicknesses and numbers of finite elements for the actuator layer. The basic shape is shown in figure 4.1 with material and geometric properties shown in table 4.1. The beam is subject to a force in the z-direction at the free end.

4.1 GAIN STUDY

This study examines the results of optimizations with different feedback gains. The actuator and sensor have been modeled using two different thicknesses, where for the thinner case one layer of finite elements represents actuator and sensor and for the thicker case two layers of finite elements are used to represent the system. Results for both cases are shown in this section.

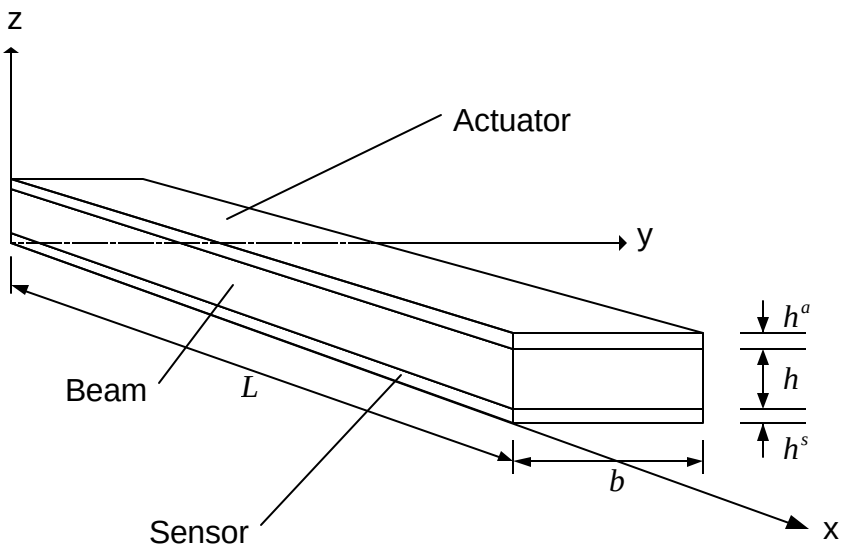

Figure 4.1 Beam used for Optimization

Table 4.1 Properties of Beam used for Optimization

Beam	
Young's Modulus	$D = 3.1028 \cdot 10^9 \frac{N}{m^2}$
Thickness	$h = 1.6 \cdot 10^{-3}\, m$
Width	$b = 0.01m$
Length	$L = 0.1m$
Poisson's ratio	$m = 0.3$
Sensor/Actuator	
Young's Modulus	$D^s = D^a = 2.00 \cdot 10^9 \frac{N}{m^2}$
Sensor/Actuator thickness Layer One-Layer Study	$h^a = h^s = 5 \cdot 10^{-4}\, m$
Sensor/Actuator thickness Layer Two-Layer Study	$h^a = h^s = 1 \cdot 10^{-3}\, m$
Dielectric constant	$p^a = p^s = 1.06481 \cdot 10^{-10} \frac{F}{m}$
Piezoelectric constant	$e^a_{311} = e^s_{311} = 0.046 \frac{V\,m}{N}$

4.1.1 ONE-LAYER GAIN STUDY

Six optimizations have been conducted using gains of 0, –150, -300, -450, -600 and –700, respectively. The goal of this optimization is, as mentioned above, to minimize the tip deflection at the free end. The optimization is constrained by the amount of material that can be used in the actuator layer. For this study, 50% of a complete filled actuator layer is the upper limit. A value less the 100% has been chosen, to get results that show a new topology. An actuator layer with 100% material will be conducted in all cases to show the best results. The start point of this optimization is a uniform actuator layer, where each material has a density of 50%, so that the constraint is not violated at the start point.

Figure 4.2 shows the geometries of optimal results for the different optimizations. The numbers above the plotted shapes give the material density in the corresponding actuator element. It is clear, that in all cases the material is moved to the left end of the beam, towards the fixed-end of the cantilever beam. This result is intuitive, since the bending moment in the beam is greatest in this area. This results in greater strain for the piezoelectric sensor and therefore also in the piezoelectric actuator. This means that in area with greater strain, greater forces are applied to reduce the strain. This is more effective then applying a control force in areas where little strain occurs, as, for example, at the free end of the beam. It is furthermore apparent that the density decreases slowly towards the free end. This result is similar to results published by Baz and Ro (1995) who showed that a tapered piezoelectric actuator has a better damping performance for active constrained layer damping materials. A tapered piezoelectric actuator corresponds

Gp = -0

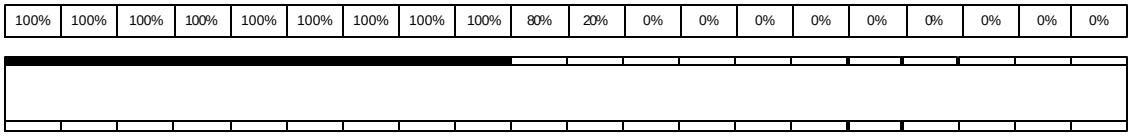

Gp = -150

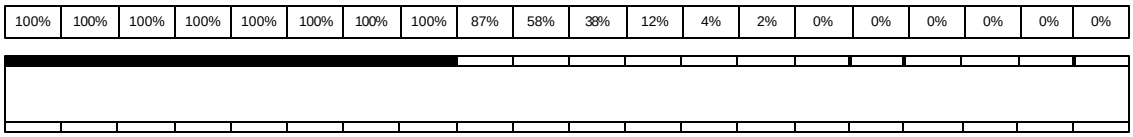

Gp = -300

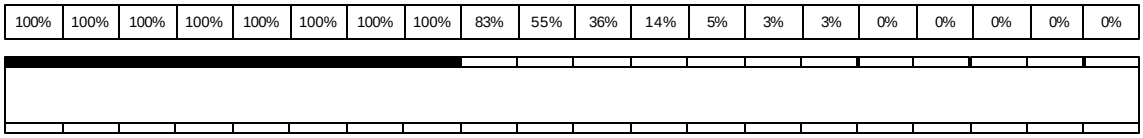

Gp = -450

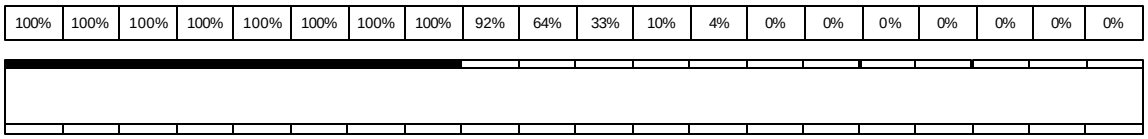

Gp = -600

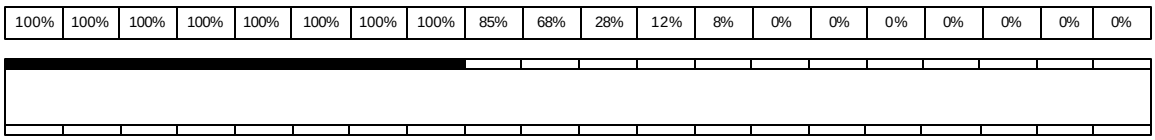

Gp = -700

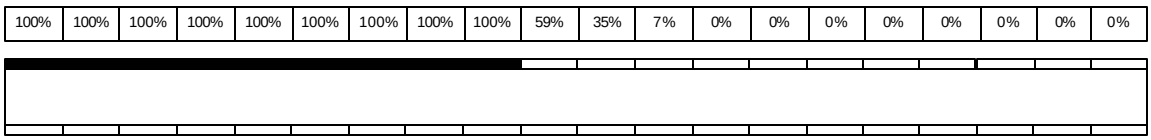

Figure 4.2 Geometries for One-Layer Gain Study

better with the linear variation of the bending moment over the length of the beam. It is therefore better, in cases where the amount of material is limited, to place some material in areas with smaller bending moments and increases the amount of material towards higher bending moments, then having a discrete layer with a discontinuity.

Figure 4.3 shows the displacement at the free end of the beam for different feedback gains and for four cases: 100% material in the actuator layer, initial point of the optimization with uniform density distribution, the optimal result and a discrete layer, where all elements at the left end of the beam have 100% density in accordance with the total density values and the remaining elements have 0% density. The case using a actuator layer with 100% material over the complete length of the beam has been chosen as a comparison, since this is the best possible configuration. This allows the determination of how an actuator with an optimal topology using less material performs in comparison to a beam using 100% material. The discrete layer has been chosen as a comparison, since it is much easier and less costly to produce.

It is apparent that the displacement varies in all cases linearly with the feedback gain. It is furthermore clear, that the tip-displacement of the beam with an actuator layer filled with 100% material is lowest, while the initial point of the optimization shows the greatest displacement for all gains. This is expected as well, since the initial point of the optimization has only 50% material in the actuator layer uniformly distributed over the beam. However, the tip-displacement of the optimal result shows similar displacements as in the case with 100% material in the actuator layer. This shows that the piezoelectric actuator is most effective in areas with high mechanical stresses, thus in this case in areas with high bending moments. The displacement of the discrete layer is nearly identical to

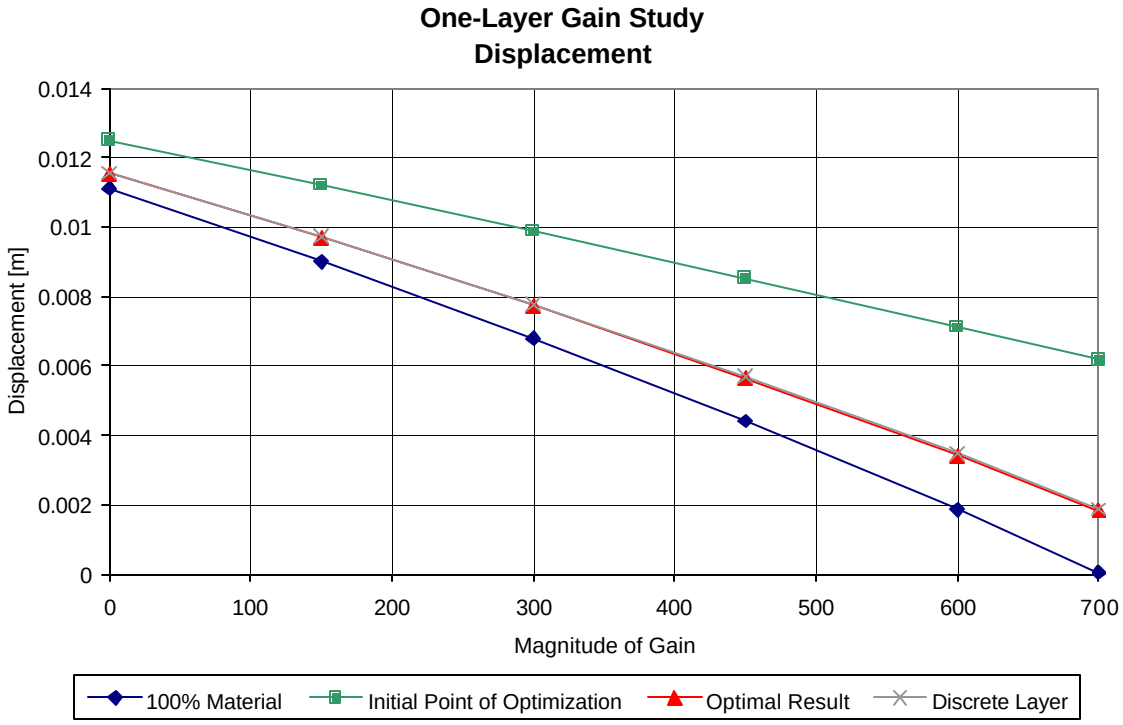

Figure 4.3 Tip Displacement of One-Layer Gain Study

the optimal result. Considering the manufacturing costs it is therefore favorable to choose a discrete layer in this case.

Figure 4.4 shows the percentage improvement of the optimal result versus the initial point, versus the discrete layer and versus a uniform actuator layer with 50% density in each element and zero gain. It is apparent that the improvement against zero gain is a linear function and shows substantial improvements. At a gain of -700 the improvement against a uniform, no gain actuator layer is 85%. The improvement between the optimal result and the initial optimization point is also substantial. At a gain of –700, an improvement of 70% against the initial point can be observed. At a gain of zero only eight percent improvement are achieved. Since no feedback control is applied, this improvement is only due to increased stiffness. It can therefore be observed, that about 60% of the improvement at a gain of –700 are obtained through the feedback control. The improvement of the optimal result versus the discrete layer is for all gains under five percent. This shows that a discrete layer has almost the same performance as mentioned above. Figure 4.5 shows a comparison of the optimal result against a uniform actuator layer with 100% material in each element. One can observe, that the displacement with 100% material is less for all gains. It can furthermore be observed, that the percentage improvement becomes worse with higher gains. This can be explained by the fact that the displacement for 100% material gets close to zero for higher gains and the percentage improvement thus gets worse.

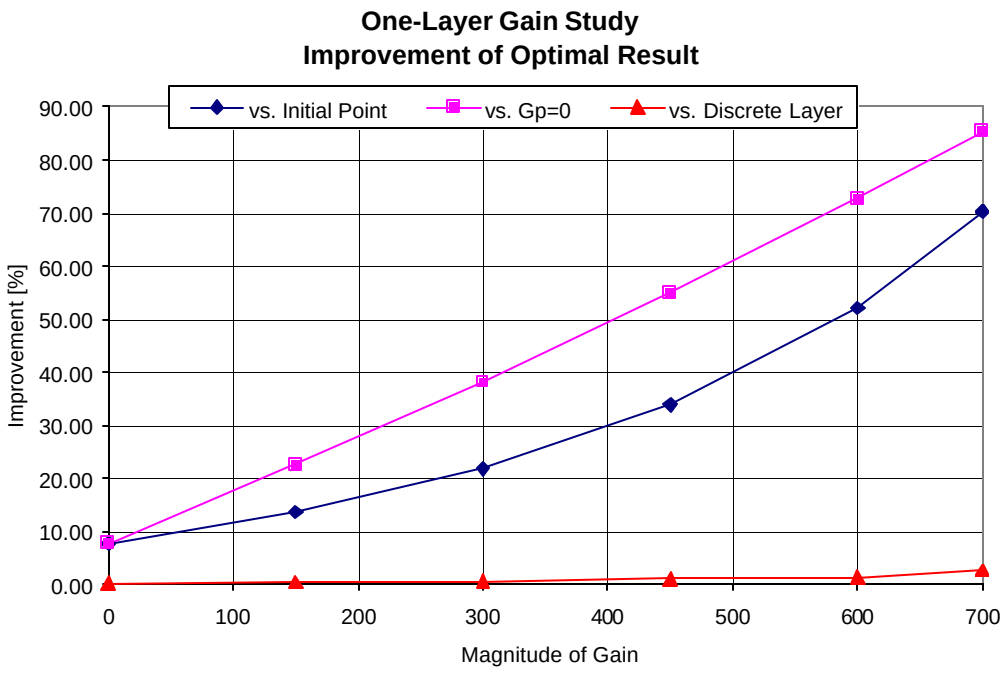

Figure 4.4 Comparison One-Layer Gain Study

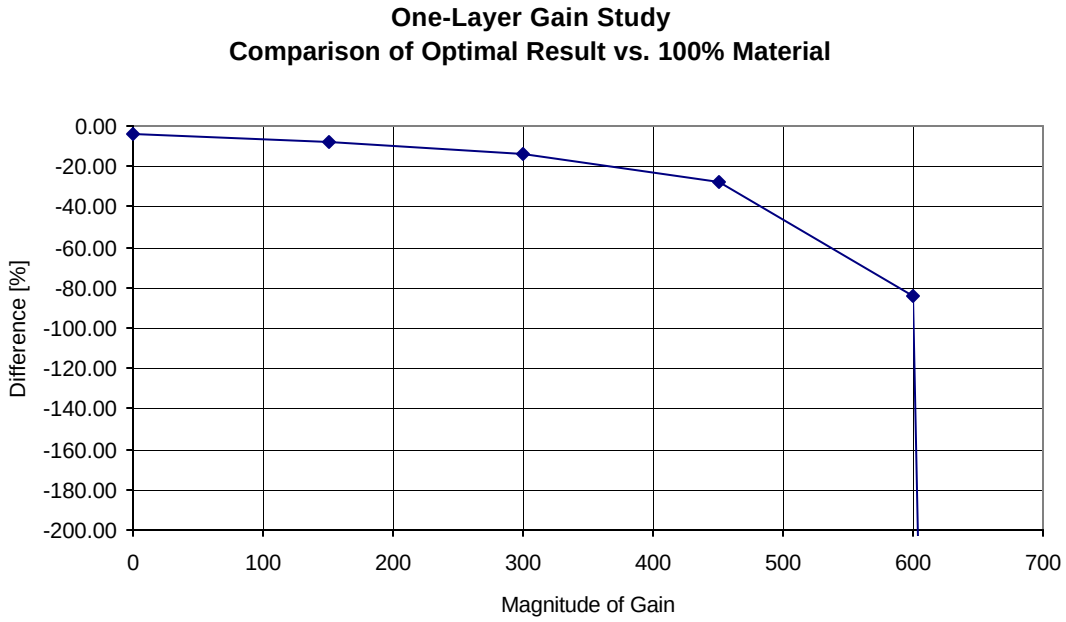

Figure 4.5 Comparison One-Layer Gain Study against 100% Material

4.1.2 TWO-LAYER GAIN STUDY

In this section the results of six optimizations are presented, where the sensor and actuator are modeled using two layers of finite elements for each. The study has been conducted using feedback gains of 0, -100, -200, -300, -350 and – 400, respectively. The optimization is constrained as described in the One-Layer case. The amount of material used for the actuator is 50% of the total material. The goal of the optimization is to minimize the tip displacement of the beam.

Figure 4.6 shows the geometries of optimal results for the different optimizations. The numbers above the plotted shape show the material density in the corresponding actuator element. It is apparent that, as in the One-Layer study, the material is concentrated on the left side of the beam, towards the fixed-end of the cantilever beam. This can be explained with the same argument stated for the One-Layer case, that the actuator is most efficient in the area with the highest bending moment. It can furthermore be observed, that the top layer has more material in the middle of the beam than the bottom layer and is connect to the base beam by materials with relative low densities. This configuration increases the moment of inertia in that area, as the moment of inertia of a thin layer in some distance from the neutral axis increases by the square of the distance, and results therefore in greater mechanical stiffness for the beam. At zero gain the optimal topology increases the stiffness of the beam of about 12% versus the initial configuration with a uniform actuator layer. Another effect of this configuration is, that the actuator force has longer moment arm to apply a counter moment, which is more significant for higher gains.

Gp=0

100%	100%	100%	100%	100%	100%	100%	100%	100%	95%	91%	58%	37%	18%	7%	8%	5%	0%	0%	0%
100%	100%	100%	100%	100%	91%	65%	27%	8%	21%	16%	16%	10%	7%	7%	8%	5%	0%	0%	0%

Gp=-100

100%	100%	100%	100%	100%	100%	100%	100%	100%	100%	95%	74%	59%	35%	22%	9%	2%	0%	0%	0%
100%	100%	100%	100%	100%	85%	50%	9%	7%	9%	7%	7%	9%	8%	7%	2%	2%	1%	1%	0%

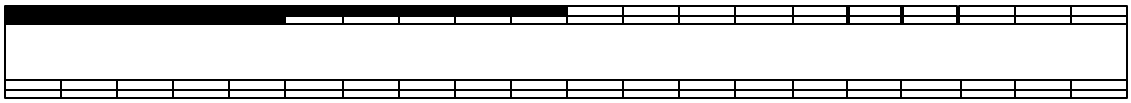

Gp=-200

100%	100%	100%	100%	100%	100%	100%	100%	100%	100%	98%	83%	57%	30%	10%	0%	0%	0%	0%	0%
100%	100%	100%	100%	100%	97%	60%	29%	9%	3%	2%	6%	4%	7%	4%	0%	0%	0%	0%	0%

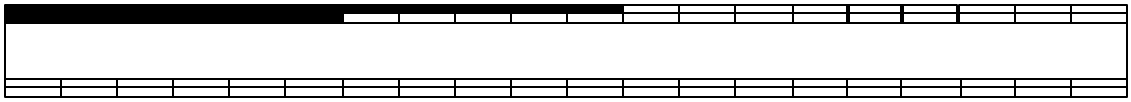

Gp=-300

100%	100%	100%	100%	100%	100%	100%	100%	100%	100%	91%	74%	59%	38%	14%	3%	1%	0%	0%	0%
100%	100%	100%	100%	100%	100%	73%	18%	23%	15%	8%	3%	3%	5%	3%	3%	1%	0%	0%	0%

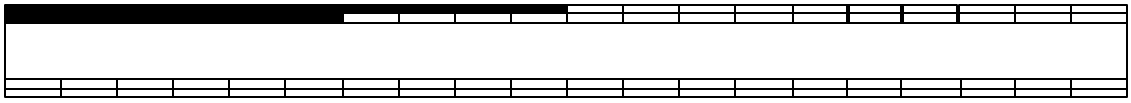

Gp=-350

100%	100%	100%	100%	100%	100%	100%	100%	100%	100%	93%	79%	49%	24%	9%	3%	0%	0%	0%	0%
100%	100%	100%	100%	100%	80%	88%	40%	35%	7%	4%	2%	8%	6%	4%	0%	0%	0%	0%	0%

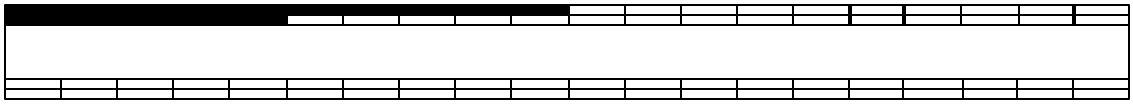

Gp=-400

100%	100%	100%	100%	100%	100%	100%	83%	83%	83%	70%	30%	16%	16%	16%	20%	0%	0%	0%	0%
100%	100%	100%	100%	100%	79%	69%	97%	0%	0%	16%	16%	20%	20%	20%	20%	20%	0%	0%	0%

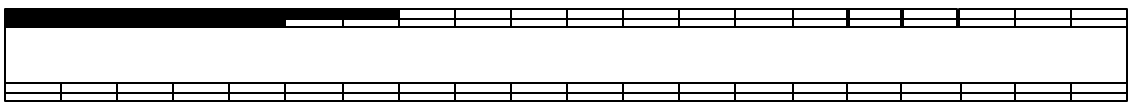

Figure 4.6 Geometries for Two-Layer Gain Study

Figure 4.7 shows the tip-displacement at the free end of the cantilever beam for different feedback gains. As in the One-Layer case, the displacements for the initial point of the optimization, the optimal result, the displacement for a discrete layer and for 100% material in the actuator layer are shown. In all three cases the tip-displacement varies linear with the feedback gain. The displacement of a beam with an actuator with 100% material over the complete length shows the lowest displacement for all gains and is therefore the best choice. However, the displacement of the optimal result is relative close to the displacement with 100% material in the actuator layer by using only 50% of the material. The displacement of the discrete layer is close to the displacement of the optimal topology, but shows slightly higher displacements for all gains. The initial point of the optimization shows the biggest displacement in this graph, which was expected, since the material is placed on the beam in an unfavorable way.

Figure 4.8 shows the percentage improvement of the optimal result versus the initial point with zero gain, versus the initial point and versus a discrete layer. Substantial improvements of up to 50% can be observed between the initial point of the optimization and the optimal result. For higher gains the optimal topology shows also a better performance compared to a discrete layer. Improvements up to 12% can be achieved, where higher gains lead to higher improvements.

Figure 4.9 shows a comparison of the tip-displacement of the optimal result versus the tip-displacement of a uniform actuator layer with 100% material in each element. It can be observed, that an actuator layer with 100% material is superior to the optimal result. The relative difference becomes bigger with higher gains. This can be explained by the fact that higher gains lead to displacement close to zero for the 100%

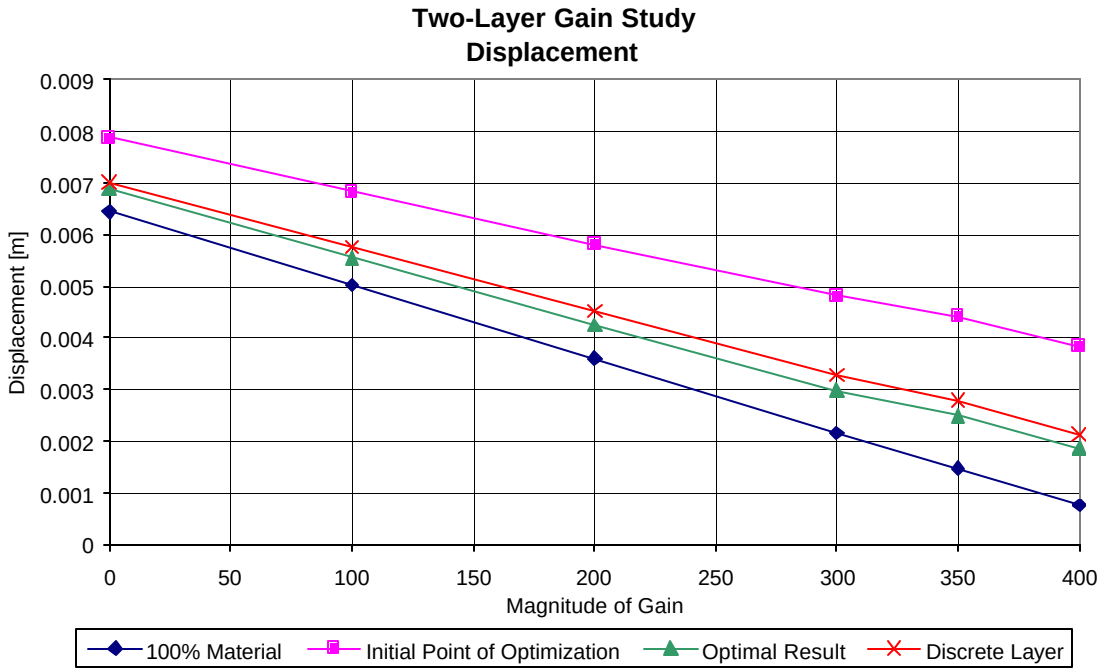

Figure 4.7 Tip Displacement of Two-Layer Gain Study

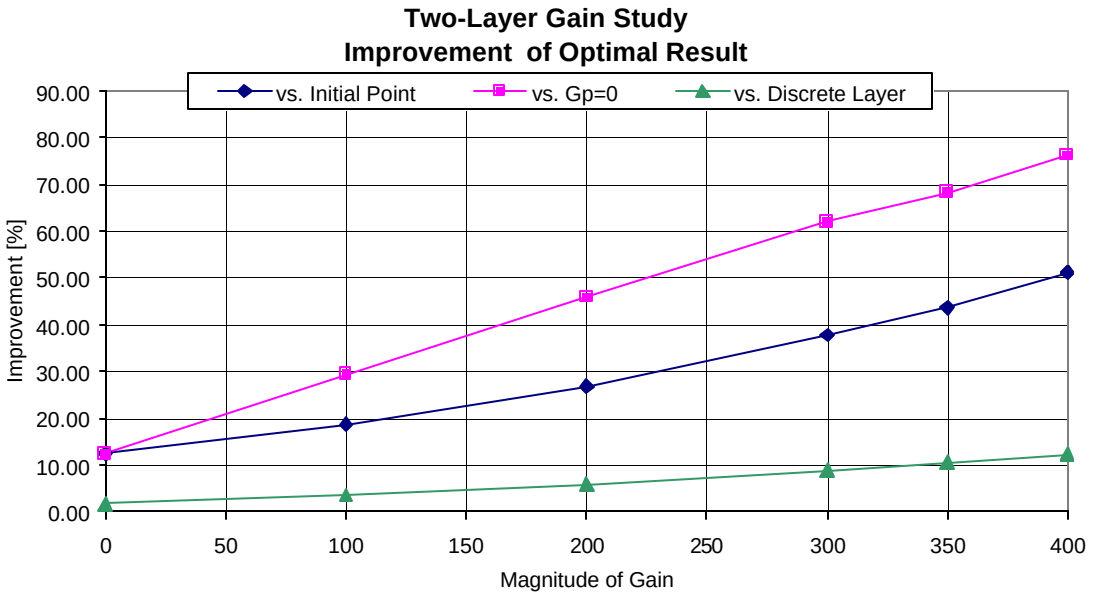

Figure 4.8 Comparison Two-Layer Gain Study

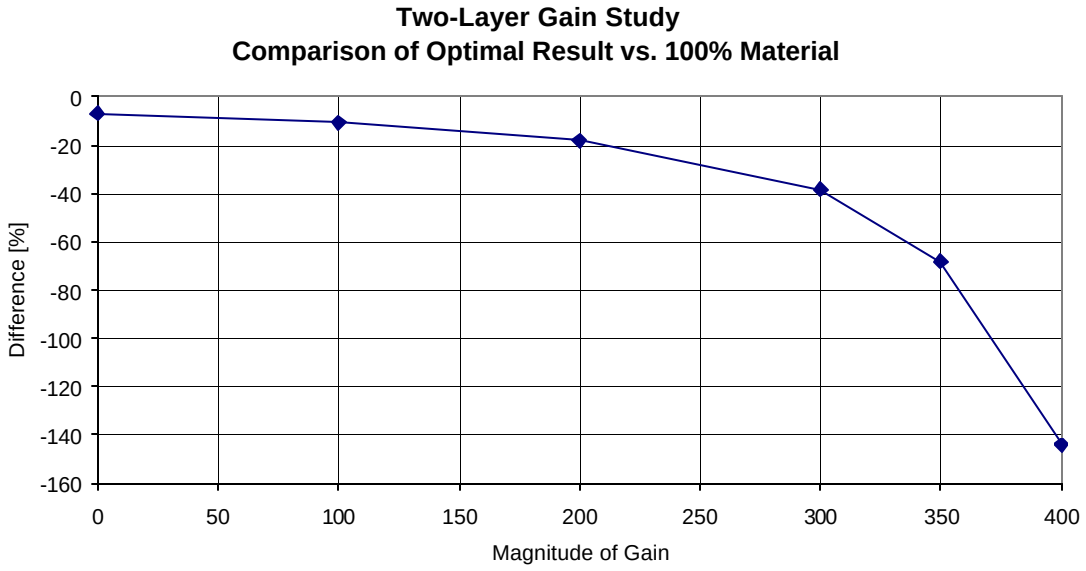

Figure 4.9 Comparison Two-Layer Gain Study against 100% Material

material case. This shows, that with only half the material satisfactory results can be achieved, if an optimal topology for the actuator is used.

4.2 DENSITY STUDY

This section examines the influence of different values of the allowed amount of material that can be used in the piezoelectric actuator. The study has been conducted, using two different thicknesses for the actuator, where the actuator has been modeled by using one or two layers of finite elements. The results of this study are presented in this section.

4.2.1 ONE-LAYER DENSITY STUDY

Six optimization results have been obtained with total density values for the actuator of 10%, 20%, 30%, 40%, 50% and 70%, respectively. The goal is to minimize the tip-deflection of the beam at the free end. All one-layer optimization results have been obtained by using a feedback gain of –600, which was determined by a trail-and-error method to get good recognizable changes in deflection by the use of a feedback gain. The start point of the optimization runs was in all cases a uniform density over the length of the actuator.

Figure 4.10 shows the geometries of the optimal results for this study. The values written above the geometry represent the density values of the corresponding finite element. It is apparent that in all cases the material tends to be concentrated to the left side of the beam, towards the fixed-end. This result corresponds with the one-layer gain

Density = 10 %

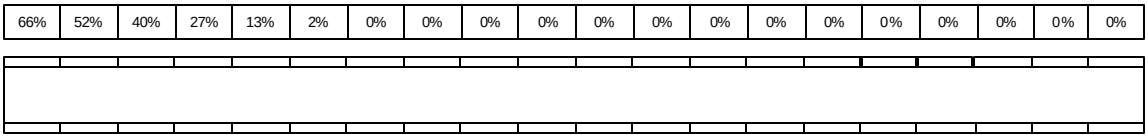

Density = 20 %

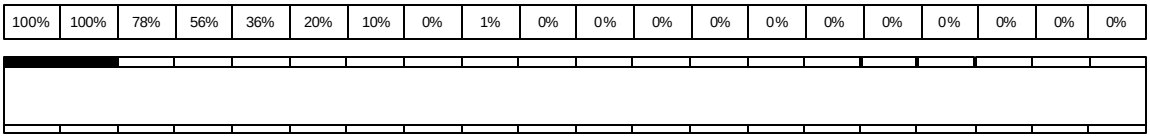

Density = 30 %

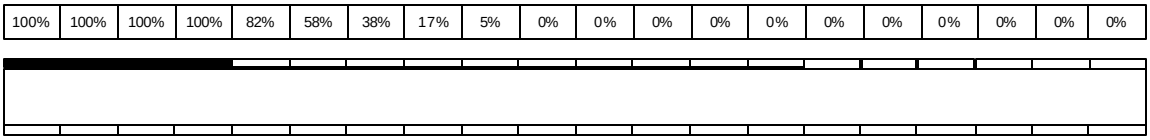

Density = 40 %

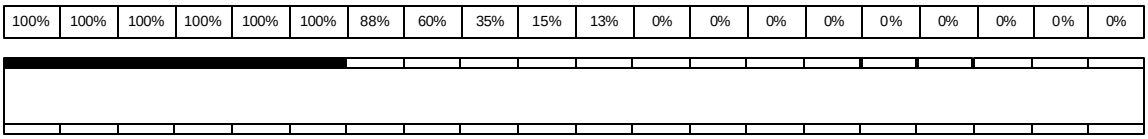

Density = 50 %

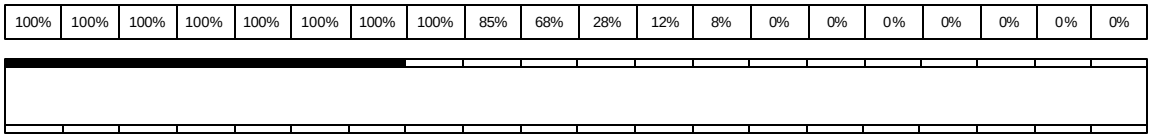

Density = 70 %

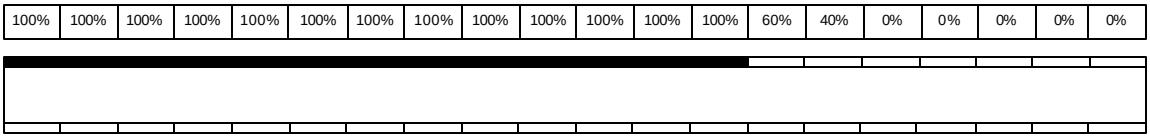

Figure 4.10 Geometries for One-Layer Density Study

study described above. The material is collected in areas with a high bending moment, which results in higher strains and makes the feedback control more effective. It can be furthermore observed, that the material decreases slowly towards the free-end. This corresponds with the results published by Baz and Ro (1995) who showed that a tapered piezoelectric actuator has a better performance in active constrained damping layers.

Figure 4.11 shows the displacement at the free end of the beam for different total density values. The displacement has been plotted for four different cases: the initial point of the optimization, the optimal result, a uniform density of the actuator layer with zero gain and a discrete layer, where all elements at the left end of the beam have 100% density in accordance with the total density values and the remaining elements have 0% density. It is apparent that the displacement for the zero gain case is greatest. The initial point of the optimization shows already substantial reduced displacement at the free end, especially for higher density values of the piezoelectric actuator. The best results can be achieved with the optimal topology defined by the optimization process or with the discrete layer, which show almost identical displacement values as the optimal result. Considering the manufacturing cost by producing a tapered piezoelectric actuator layer, the discrete layer is the better choice since it is much easier to manufacture. Figure 4.11 shows furthermore, that using only 50% of material for the actuator layer in a optimal way, results in nearly as good displacements as using an actuator layer over the complete length. This consideration can save costs by using only half of the material.

Figure 4.12 shows the improvement of the optimal result versus the uniform layer with zero gain, versus the initial point of the optimization and versus the discrete layer. One can see that the optimal result shows more improvement versus the initial point of

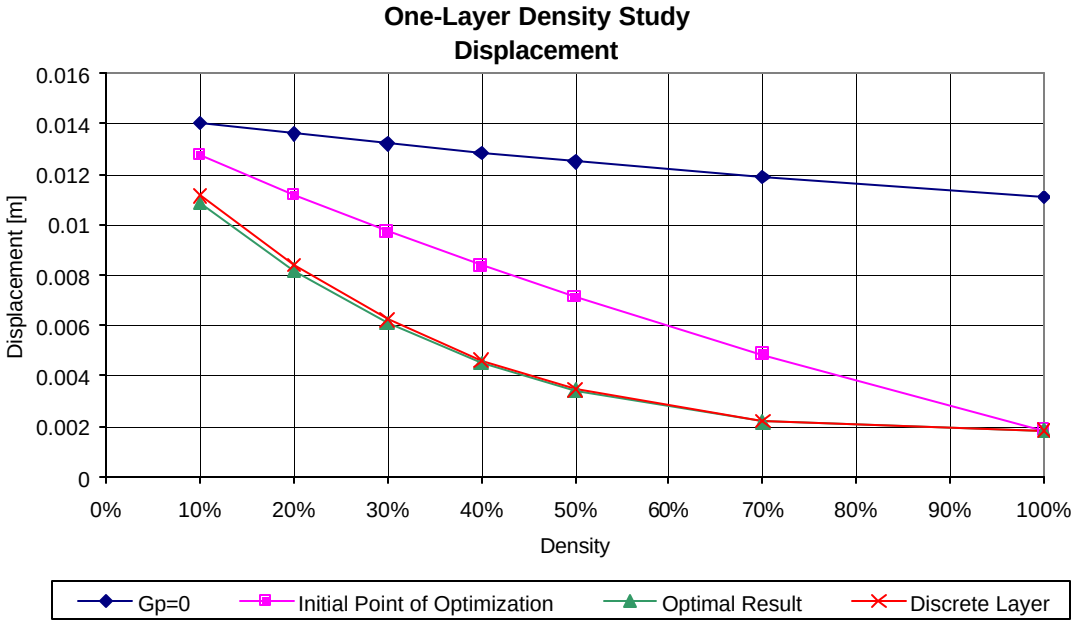

Figure 4.11 Tip Displacement of One-Layer Density Study

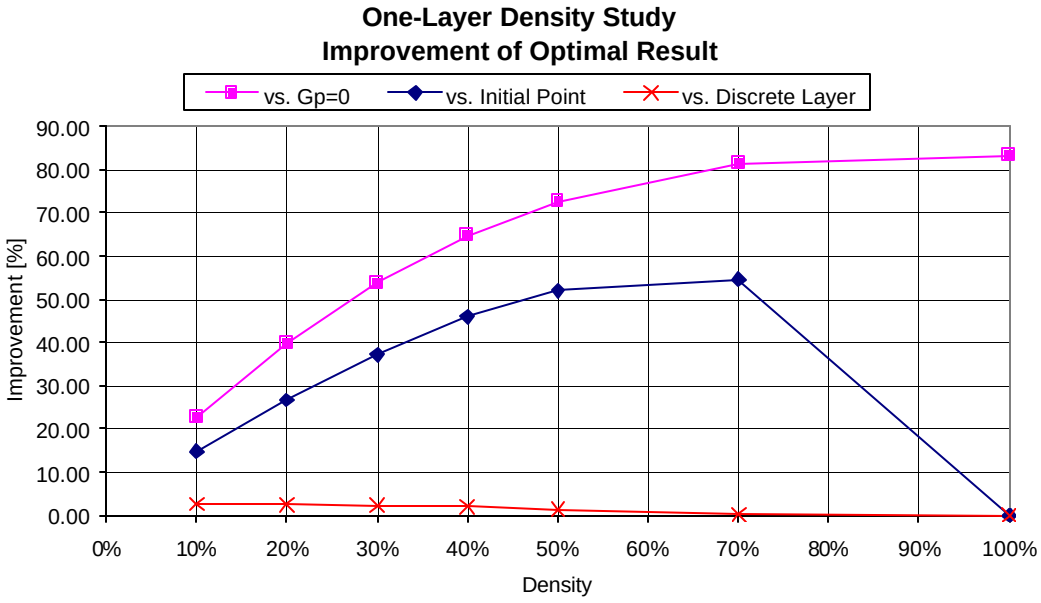

Figure 4.12 Comparison One-Layer Density Study

the optimization and versus a uniform actuator with zero gain with increasing density values. A maximal point of improvement of the optimal result versus the initial point of the optimization is reached at about 70% total density for the actuator. This shows that adding more material to the actuator layer does not substantially improve the performance. Using more material than 70% of the total material will result in more material towards the free end of the beam. Since the bending moment is relatively small in that area, almost no control force is applied. The material is therefore not as efficient. It has furthermore been shown that tapering the end of the piezoelectric actuator increases its performance. By adding more material to the free end of the beam, it might not be possible to taper the actuator and a loss in the percentage of improvement is the consequence. A total density value of 70% for the actuator shows the best efficiency for the material used.

Figure 4.13 shows a comparison of the optimal result versus a uniform actuator layer with 100% material in each element. One can observe that the actuator layer with 100% material has a better performance then the actuator layers with less density. However, the optimal result using a total density value of 70% shows a difference of only 18%. Depending on the actual application, this might be good enough to stiffen the structure. Thus, less material can be used and a good performance can be achieved at less cost.

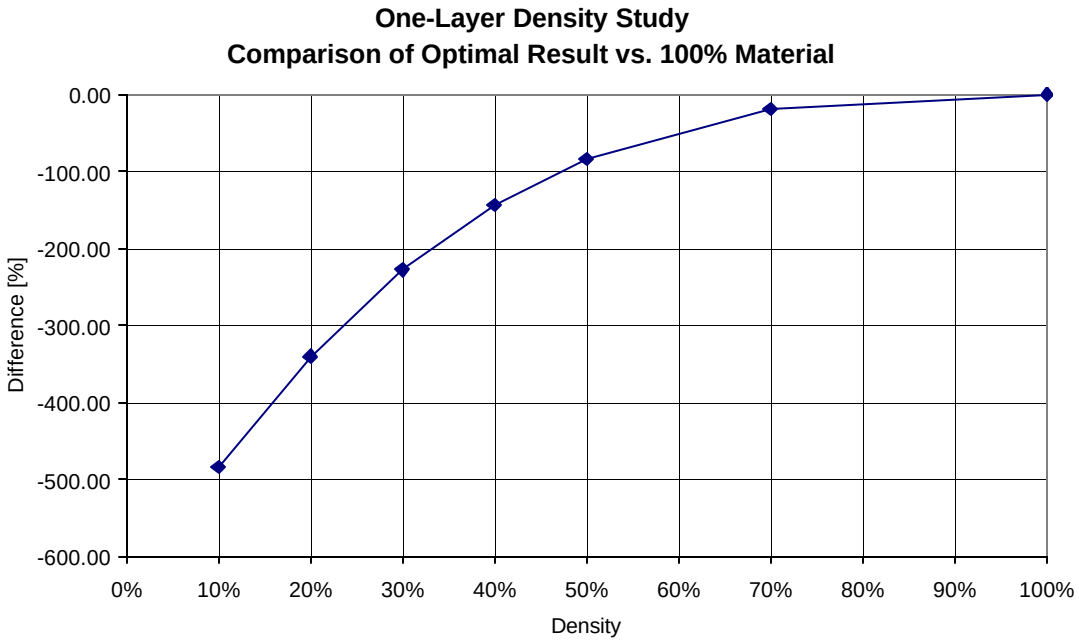

Figure 4.13 Comparison One-Layer Density Study against 100% Material

4.2.2 TWO-LAYER DENSITY STUDY

Six optimizations have been conducted with total density values for the actuator of 10%, 20%, 30%, 40%, 50% and 70%, respectively. The goal is to minimize tip-deflection of the beam at the free end. All optimizations have been conducted by using a feedback gain of –350 which has been determined by a trial-and-error method to get recognizable deflection changes by using the feedback gain. The start point of the optimizations was in all cases a uniform density over the length of the actuator.

Figure 4.14 shows the geometries of the optimal results for the different optimizations. The number above the plotted shape shows the material density in the corresponding actuator element. It is again apparent that the material is concentrated on the left side of the beam, towards the fixed-end. The same explanation as before can be given: the actuator is most efficient in areas with a high bending moment. It can furthermore be observed, as in the two-layer gain study, that the top layer has more material then the bottom layer. Depending on the total density value for the optimization, in some cases only the top layer has elements filled with 100% material, whereas the bottom layer has elements with relatively low density values. This can also be explained as in the Two-Layer gain study case with two facts: the increase moment of inertia and the longer moment arm for the control force. For further details of the explanation, please refer to the Two-Layer gain study section.

Figure 4.15 shows the displacement at the free end of the beam for different total density values. The displacement has been plotted for four different cases: the initial point of the optimization, the optimal result, a uniform density of the actuator layer with

Density=10%

71%	71%	58%	53%	44%	33%	23%	16%	6%	3%	1%	1%	0%	0%	0%	0%	0%	0%	0%	0%
0%	0%	4%	2%	2%	3%	1%	1%	2%	0%	0%	0%	0%	0%	0%	0%	0%	0%	0%	0%

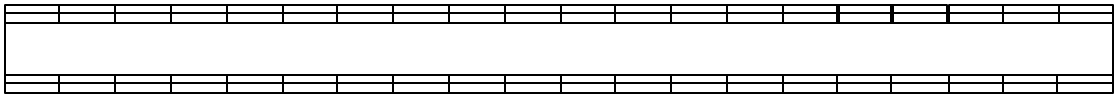

Density=20%

100%	100%	100%	96%	87%	68%	61%	46%	40%	26%	11%	8%	3%	0%	0%	0%	0%	0%	0%	0%
8%	7%	4%	3%	3%	8%	1%	7%	1%	6%	5%	1%	1%	0%	0%	0%	0%	0%	0%	0%

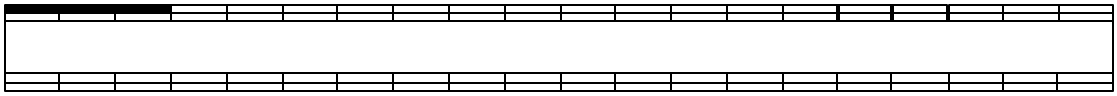

Density=30%

100%	100%	100%	100%	100%	100%	98%	82%	62%	52%	37%	23%	9%	3%	0%	0%	0%	0%	0%	0%
87%	70%	35%	12%	3%	2%	2%	4%	6%	2%	4%	3%	3%	0%	0%	0%	0%	0%	0%	0%

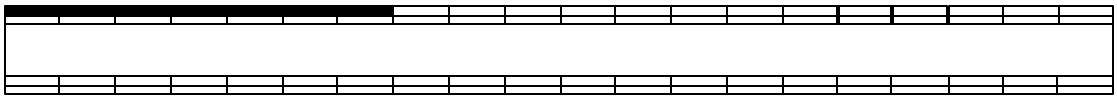

Density=40%

100%	100%	100%	100%	100%	100%	100%	100%	95%	76%	55%	42%	21%	9%	9%	1%	0%	0%	0%	0%
100%	100%	100%	86%	54%	22%	19%	5%	3%	6%	9%	8%	5%	1%	1%	0%	0%	0%	0%	0%

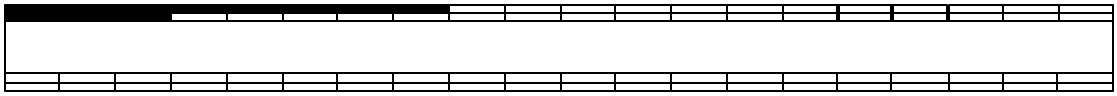

Density=50%

100%	100%	100%	100%	100%	100%	100%	100%	100%	100%	93%	79%	49%	24%	9%	3%	0%	0%	0%	0%
100%	100%	100%	100%	100%	81%	88%	40%	4%	7%	5%	3%	8%	6%	4%	0%	0%	0%	0%	0%

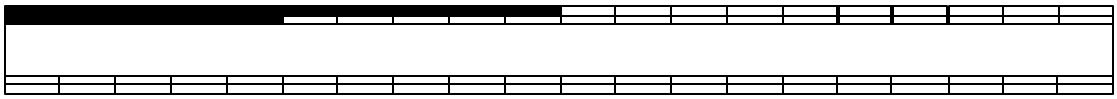

Density=70%

100%	100%	100%	100%	100%	100%	100%	100%	100%	100%	100%	100%	100%	100%	74%	48%	17%	0%	0%	0%
100%	100%	100%	100%	100%	100%	100%	100%	100%	100%	100%	100%	63%	4%	4%	2%	7%	0%	0%	0%

Figure 4.14 Geometries for Two-Layer Density Study

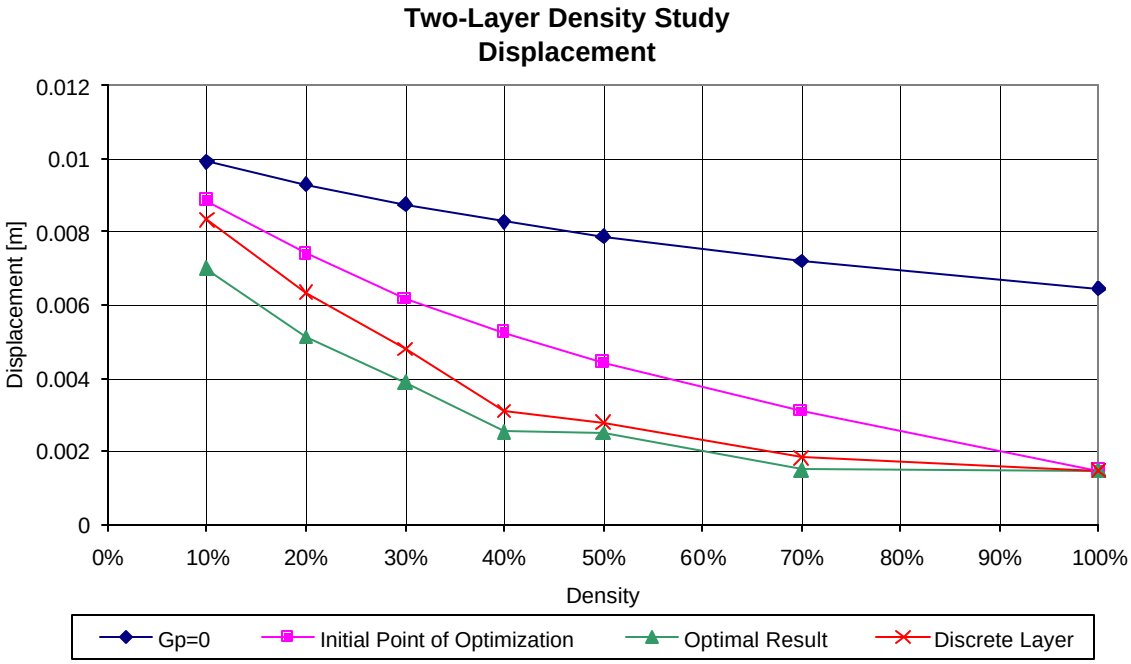

Figure 4.15 Tip Displacement of Two-Layer Density Study

zero gain and for a discrete layer. It is apparent that the displacement for the zero gain, as in the one-layer density study, case is greatest. The initial point of the optimization shows already substantially reduced displacement at the free end, especially for higher density values of the piezoelectric actuator. The best results can be achieved with the optimal topology defined by the optimization process. The displacement of the discrete layer, where all elements at the at the left side of the beam are filled with 100% material in accordance with the total density value, shows also low displacement values. However, the results shown as best topologies are recognizably better, especially for lower density values. The displacement of the optimal result with a total density value of 50% seems to be a little too high, as until now all curves showed a smooth behavior. For this reason, the second optimization for this point has been conducted using a smaller finite difference step size and tighter convergence tolerances. The result of the second optimization confirmed the result shown here.

Figure 4.16 shows the improvement of the optimal result versus the uniform layer with zero gain, versus the initial point of the optimization and versus the discrete layer. As in the previous studies the improvement of the optimized result versus a case without a control force shows the greatest improvement. This is intuitive, since no feedback control is applied to reduce the deflection. The improvement of the optimal result versus the initial point of the optimization shows a maximal improvement in the area between 40% and 60% total density values. This can be explained as in the one-layer density study case, that more material towards the free end of the beam has less influence on the stiffness of the system, reduces however the possibility to taper the piezoelectric actuator. The comparison between the optimal result and the discrete calculation shows, that a

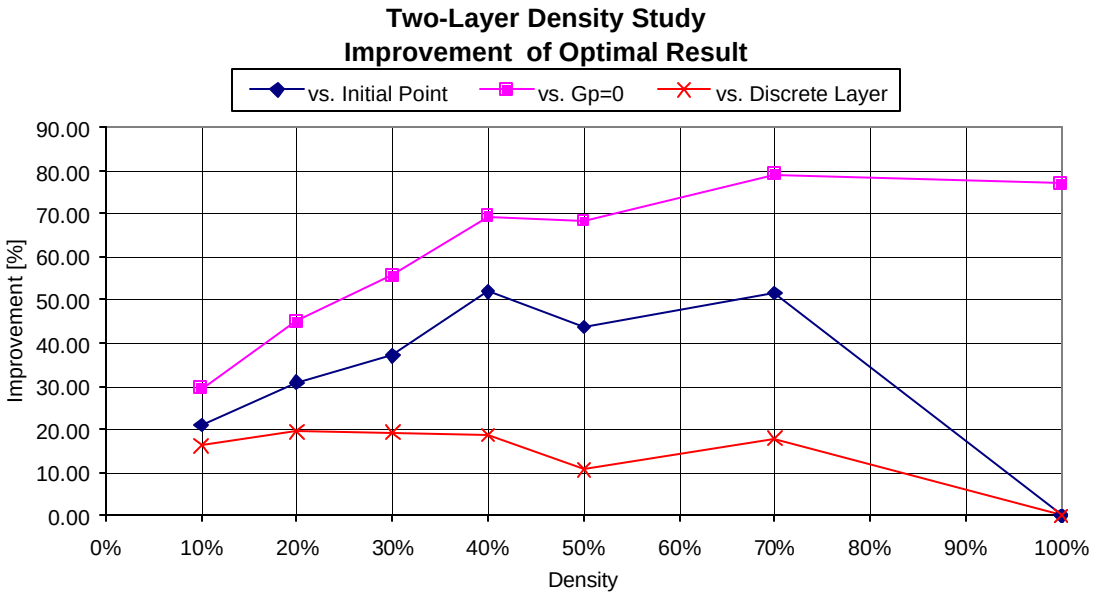

Figure 4.16 Comparison Two-Layer Density Study

tapered actuator with more material concentrated in the top layer has a about 20% better performance than the discrete layer.

Figure 4.17 shows a comparison of the tip-deflection of the optimal result versus the tip-deflection with an actuator layer with 100% material. It is apparent, that the actuator with 100% total material density has a better performance then all actuators with less material density. However, with increasing total density used for the actuator, the comparison shows that the difference becomes much smaller. At 70% total material density, the case with 100% material density shows only a better performance of one percent. This is relatively small and shows, that nearly the same performance can be achieved by using only 70% material.

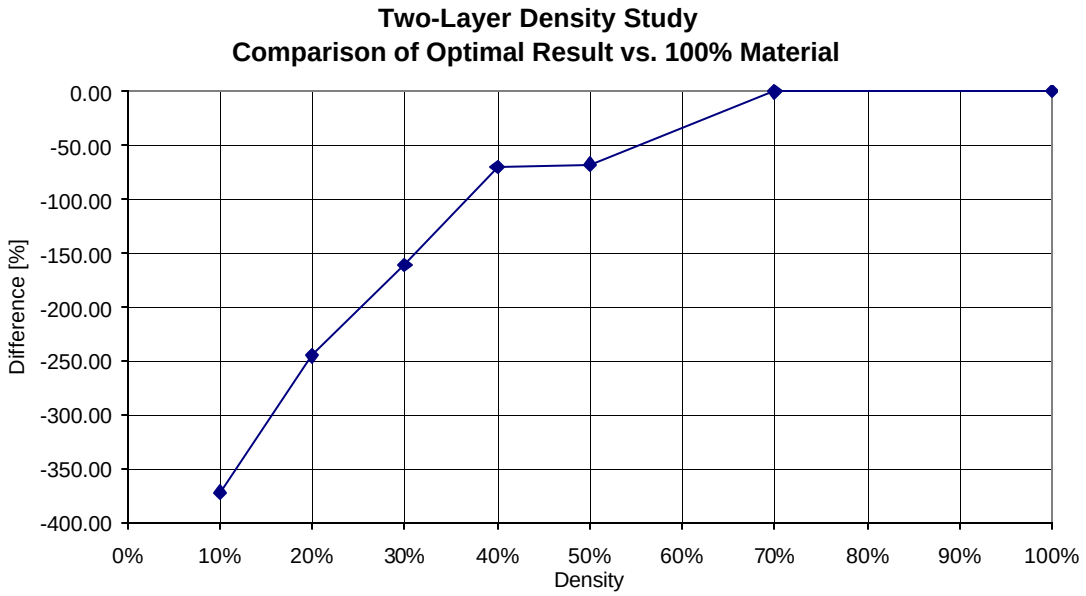

Figure 4.17 Comparison Two-Layer Density Study against 100% Material

5 CONCLUSION AND FUTURE WORK

A feedback control law for static calculations has been implemented in the commercial finite element program ABAQUS. This has been done through a modification of the stiffness matrices, which are assembled in ABAQUS. The result of the finite element calculation has been verified with analytic solutions. It has been attempted to implement proportional and derivative feedback control for a steady state dynamic calculation without achieving satisfactory results.

The finite element calculation has been linked with the commercial optimization algorithm VisualDOC and a parameter study has been conducted. The parameter study examined the influence of different feedback gains and total density values on the result of the optimization. Two different thicknesses for the piezoelectric actuator have been used and have been modeled using one or two layers of piezoelectric elements, respectively.

The results of the optimization showed substantial improvement compared to the initial optimization configuration. It has, furthermore, been shown that 70% of the total actuator material is enough to achieve nearly the same performance as with 100% material. The optimized topology is intuitive for the case where the actuator has been modeled with one layer of piezoelectric material. The material is collected in areas with a high bending moment, where the actuator shows the best performance. Improvements of up to 70% could be achieved, comparing the staring point and the ending point of the optimization. Comparison of the optimal topology against a discrete layer showed only a performance increase of maximal 5%, which might not be enough considering the higher manufacturing costs. Non-intuitive topologies are discovered for optimizations, where

the actuator has been modeled using two piezoelectric element layers. Reasonable physical explanations have been found which explain the topologies found. It could also be observed that the material is collected in areas with high bending moments, but more material has been collected in the top layer, which was connected to the base beam by low-density elements. Improvements of up to 50% could be achieved, comparing the initial point and the optimal results of the optimization. A comparison with the results of a discrete layer showed that the optimal result has an up to 20% better performance, which may be enough to justify higher manufacturing costs.

Given more time, future studies could easily be extended by studying other geometries, boundary conditions or initial optimization points. For example, a simply supported beam could be studied with a force applied in the middle of the beam. More layers of piezoelectric elements could be used to model the actuator and the influence on the result of the optimization could be examined. It is furthermore possible to give a non-uniform density distribution as initial point of the optimization, and to examine the results of these optimizations. Since all optimizations in this study have been conducted by using a node-to-node control, future work could show how the results differ if an optimization is conducted using a layer-to-layer control law. It is furthermore possible to implement a penalty function in the optimization setup, which forces all elements to be either 100% material or to be void. A parameter study, as done in this study, can be conducted to get a deeper understanding of this area.

Even more research time would be necessary to continue the research of the implementation of proportional and derivative feedback control for a steady state

dynamic calculation. A verification of this work would lead to optimizations using that finite element model and determining the best topology for maximal vibration damping. Another parameter study could be conducted using the steady state implementation of the control laws, as it has been done for the static case in this study. Another method of damping could be implemented, as, for example, structural damping, and the effects on the optimization could be examined. Another aspect of this kind of optimization is the influence of the control law. Different control algorithms could be implemented and the influence of them to the result of an optimization could be examined.

After completion of this study, an optimization including piezoelectric and viscoelastic material could be conducted, to get topologies such as an active constrained layer damping (ACLD) structure (Lumsdaine 2001). The goal of this optimization would be to determine the best topology of these two materials, which leads to the best topology for active constrained layer damping.

For all described future work a comparison with experimental results could be done, to get a better verification of the analytic or FEM solutions. An idea for manufacturing such shapes is given through Bandyopadhyay et al. (1997) who describe a fused deposition technique for piezocomposites.

REFERENCES

References

Allaire, G. (2002). Shape Optimization by the Homogenization Method. New York, Springer.

Bandyopadhyay, A., R. K. Panda, et al. (1997). "Processing of Piezocomposites by Fused Deposition Technique." Journal of the American Ceramic Society **80**(6): 1366-1372.

Baz, A. and J. Ro (1995). "Performance-Characteristics of Active Constrained Layer Damping." Shock and Vibration **2**(1): 33-42.

Bendsoe, M. P. and N. Kikuchi (1988). "Generating Optimal Topologies in Structural Design Using a Homogenization Method." Computer Methods in Applied Mechanics and Engineering **71**(2): 197-224.

Buehler, M., B. Bettig, et al. (2002). "Topology Optimization of Smart Structures using a Homogenization Approach". Proceedings, SPIE Smart Structures and Materials, San Jose, CA.

Chang, W., S. V. Gopinathan, et al. (2002). "Design of Robust Vibration Controller for a Smart Panel Using Finite Element Model." Journal of Vibration and Acoustics-Transactions of the ASME **124**(2): 265-276.

Gabbert, U., H. Köppe, et al. (2002). "Controller Design for Engineering Smart Structures Based on Finite Element Models". Proceedings, SPIE Smart Structures and Materials, San Jose, CA.

Gaudenzi, P., R. Carbonaro, et al. (2000). "Control of Beam Vibrations by Means of Piezoelectric Devices: Theory and Experiments." Composite Structures **50**(4): 373-379.

Guyan, R. J. (1965). "Reduction of Stiffness and Mass Matricies." AIAA Journal **3**(2): 380.

Ha, S. K., C. Keilers, et al. (1992). "Finite-Element Analysis of Composite Structures Containing Distributed Piezoceramic Sensors and Actuators." AIAA Journal **30**(3): 772-780.

Han, J. H., K. D. Cho, et al. (1999). "Vibration and Actuation Characteristics of Composite Structures with a Bonded Piezo-Ceramic Actuator." Smart Materials & Structures **8**(1): 136-143.

Hassani, B. A. and S. G. Hinton (1999). Homogenization and Structural Topology Optimization : Theory, Practice, and Software. New York, Springer Verlag.

Hibbit, Karlsson, et al. (2002). ABAQUS/Standard User's Manual.

Hossack, J. A. and G. Hayward (1991). "Finite-Element Analysis of 1-3 Composite Transducers." IEEE Transactions on Ultrasonics Ferroelectrics and Frequency Control **38**(6): 618-629.

Kim, J., V. V. Varadan, et al. (1996). "Finite-Element Modeling of a Smart Cantilever Plate and Comparison with Experiments." Smart Materials & Structures **5**(2): 165-170.

Kim, J., V. V. Vardan, et al. (1997). "Finite Element Modeling of Structures Including Piezoelectric Active Devices." International Journal for Numerical Methods in Engineering **40**: 817-832.

Lerch, R. (1990). "Simulation of Piezoelectric Devices by 2-Dimensional and 3-Dimensional Finite-Elements." Ieee Transactions on Ultrasonics Ferroelectrics and Frequency Control **37**(3): 233-247.

Loveday, P. W. (2002). "Comparison of Amplified Piezoelectric Actuators Based on Topological Optimization". Proceedings, SPIE Smart Structures and Materials, San Jose, CA.

Lumsdaine, A. (2001). "Modeling of Active Constrained Layer Damping Structures Using a commercial Finite Element Code". ASME International Mechanical Engineering Congress and Exposition, New York, NY.

Lumsdaine, A. (2002). "Topology Optimization of Constrained Damping Layer Treatments". ASME International Mechanical Engineering Congress & Exposition, New Orleans, LA.

Naillon, M., R. H. Coursant, et al. (1983). "Analysis of Piezoelectric Structures by a Finite-Element Method." Acta Electronica **25**(4): 341-362.

Papalambros, P. Y. and J. W. Douglas (2000). Principles of Optimal Design. Cambridge, Cambridge University Press.

Sigmund, O. and S. Torquato (1997). "Design of Materials with Extreme Thermal Expansion Using a Three-Phase Topology Optimization Method." Journal of the Mechanics and Physics of Solids **45**(6): 1037-1067.

Silva, E. C. N., J. S. O. Fonseca, et al. (1999). "Design of Piezocomposite Materials and Piezoelectric Transducers Using Topology Optimization - Part I." Archives of Computational Methods in Engineering **6**(2): 117-182.

Silva, E. C. N., J. S. O. Fonseca, et al. (1997). "Optimal Design of Piezoelectric Microstructures." Computational Mechanics **19**(5): 397-410.

Silva, E. C. N., J. S. O. Fonseca, et al. (1998). "Optimal Design of Periodic Piezocomposites." Computer Methods in Applied Mechanics and Engineering **159**(1-2): 49-77.

Silva, E. C. N. and N. Kikuchi (1999). "Design of Piezocomposite Materials and Piezoelectric Transducers Using Topology Optimization - Part III." Archives of Computational Methods in Engineering **6**(4): 305-329.

Silva, E. C. N. and N. Kikuchi (1999). "Design of Piezoelectric Transducers Using Topology Optimization." Smart Materials & Structures **8**(3): 350-364.

Silva, E. C. N., S. Nishiwaki, et al. (1999). "Design of Piezocomposite Materials and Piezoelectric Transducers Using Topology Optimization - Part II." Archives of Computational Methods in Engineering **6**(3): 191-222.

Silva, E. C. N., S. Nishiwaki, et al. (2000). "Topology Optimization Design of Flextensional Actuators." IEEE Transactions on Ultrasonics Ferroelectrics and Frequency Control **47**(3): 657-671.

Tzou, H.-S. (1993). Piezoelectric Shells. Boston, Kluwer Academic.

Tzou, H. S. and C. I. Tseng (1990). "Distributed Piezoelectric Sensor / Actuator Design for Dynamic Measurement / Control of Distributed Parameter-Systems - A Piezoelectric Finite-Element Approach." Journal of Sound and Vibration **138**(1): 17-34.

Tzou, H. S. and C. I. Tseng (1991). "Distributed Modal Identification and Vibration Control of Continua - Piezoelectric Finite-Element Formulation and Analysis."

Journal of Dynamic Systems Measurement and Control-Transactions of the ASME **113**(3): 500-505.

Varadan, V. V., Y. H. Lim, et al. (1996). "Closed Loop Finite-Element Modeling of Active/Passive Damping in Structural Vibration Control." Smart Materials & Structures **5**(5): 685-694.

Veley, D. E. and S. S. Rao (1996). "A Comparison of Active, Passive and Hybrid Damping in Structural Design." Smart Materials & Structures **5**(5): 660-671.

Yi, Y. M., S. H. Park, et al. (2000). "Design of Microstructures of Viscoelastic Composites for Optimal Damping Characteristics." International Journal of Solids and Structures **37**(35): 4791-4810.

APPENDIX

A APPENDIX A SURVEY OF SEVEN NON-LINEAR CONSTRAINED OPTIMIZATION PROGRAMS

A.1 INTRODUCTION

This paper gives an overview of seven non-liner constrained optimization programs. The programs are described, evaluated for ease of use, compatibility to combine with other programs and numerical accuracy. A fact sheet listing process and contact dresses is shown in table A.1. Three example problems are calculated with each program. A qualitative ranking is introduced for ease of use and a quantitative ranking is done for the results of the optimization. Finally, both rankings are combined and the optimization programs are compared over the overall performance. A recommendation for new software purchase is given.

A.2 DESCRIPTION OF THE EVALUATED OPTIMIZATION CODES

First a short overview of the evaluated software is given. For each program the features and the optimization used algorithm are mentioned. In this part no judgment of the software is given.

A.2.1 LINGO

Lingo is a Design tool for solving linear, nonlinear and integer optimization problems. The primary optimization technique used by the nonlinear solver is based upon a Generalized Reduction Gradient (GRG) algorithm. It is also possible to include other algorithms into the optimization, for example a crash procedure, a Steepest Edge/Steepest

Table A.1 Program fact sheet

Program	Solver	Price (annual)	Price (purchase)	Variables	Constraints	Manual	OP Systems	Email	Homepage
Lingo	GRG, SQP	--	$320	200	1000	500 Pages	Windows, Linux, Solaris	webinfo@lindo.com	www.lindo.com
Matlab	SQP	--	$200	N/A	N/A	332 Pages	Windows, Linux, Solaris	service@mathworks.com	www.mathworks.com
NLPQL	SQP	N/A	N/A	N/A	N/A	N/A	All (source code)	N/A	N/A
EPOGY	SQP, Downhill Simplex, Genetic	--	$1,980	200 & more	N/A	138 Pages	Windows, Linux, SGI	biz@synaps-inc.com	www.synaps-inc.com
OptdesX	GRG, SQP	N/A	N/A	N/A	N/A	197 Pages	Unix	N/A	N/A
VisualDOC	SLP, SQP, MMFD	$750	$1,875	N/A	N/A	172 Pages	Windows, Unix	sales@vrand.com	www.vrand.com/

Decent option, and Sequential Linear Programming. The solver will automatically select the solution approach that appears best suited to the specific model at hand. The solution approach is dynamically adjusted during the solution process based upon the model's behavior.

The optimization model must be enterd with a particular syntax, but does not need to be presented in a defined form (e.g. negative null form). It is furthermore possible to read data from other applications into LINGO or start other applications from LINGO.

A.2.2 MATLAB

The Optimization Toolbox extends the MATLAB environment to provide tools for both general and large-scale optimization of nonlinear functions. Additional tools, including large-scale methods, are provided for linear programming, quadratic programming, nonlinear least squares, and solving nonlinear equations. The optimization algorithm used for constraint non-linear optimization problem is sequential quadratic programming (SQP).

Optimization routines can be very easily integrated into existing Matlab programs. Since Matlab is capable of running other programs out of the Matlab environment, it is possible to build complex optimizations including other programs.

A.2.3 NLPQL

NLPQL solves general nonlinear mathematical programming problems with equality and inequality constraints. The internal algorithm is a sequential quadratic

programming (SQP) method. NLPQL is written in double precision FORTRAN-77 and organized in form of a subroutine. Nonlinear problem functions and analytical gradients must be provided by the user within special subroutines or the calling program. This allows a great flexibility, since the program is accessible in the source code and modifications can be made easily.

A.2.4 EPOGY

Epogy is a program package that allows creating a complex optimization analysis within one program. Epogy runs the analysis software, reads the required data out of the result files, runs the optimization algorithm and returns the new values for the design variables to the analysis software.

The optimization algorithms used for non-linear problems are sequential quadratic programming, downhill-simplex, a genetic algorithm and a Monte-Carlo optimization. The user is not required to have much knowledge over optimization or the algorithm, since Epogy tries to figure out what the best suited algorithm for the given problem is.

A.2.5 OPTDESX

OptdesX is an interactive computer program for computer-aided optimization and design. It has been developed to address the needs of an engineer in a design environment. OptdesX allows the user, for example, to optimize with both continuous and discrete variables, including components from vendor catalogs, and redefine a design problem very quickly using point and click operations.

For solving optimization problems containing continuous variables OptdesX offers a Generalized Reduction Gradient (GRG) algorithm and a Sequential Quadratic Programming (SQP) algorithm. Furthermore, the following algorithms for mixed integer or discrete problems are included in this program package:

- Branch and Bound
- Simulated Annealing
- Exhaustive Search

A.2.6 VISUALDOC

VisualDOC is a general-purpose numerical optimization software package, which can be used to solve a wide variety of nonlinear optimization problems. The user provides a main program for calling VisualDOC and an analysis program to evaluate the necessary functions. VisualDOC is linked with the user's codes to create the design optimization program. VisualDOC will change the input parameters to the analysis in order to minimize or maximize the user-defined objective, subject to constraints (limits) on other user-defined responses. To achieve this, VisualDOC calls the analysis program repeatedly while searching for the optimum.

For a constrained non-linear optimization problem, there are three algorithms are available, Modified Method of Feasible Directions (MMFD), Sequential Linear Programming (SLP) and Sequential Quadratic Programming (SQP). VisualDOC offers furthermore two optimization algorithms for non-gradient based optimizations that are Particle Swarm Optimization (PSO) and a genetic algorithm. For mixed integer or

discrete problems the Design of Experiments and Response Surface algorithms are available.

A.2.7 SOLVER DLL

The Solver DLL program package allows the user to develop custom applications, which may run on C/C++, Visual Basic or another Windows programming language. According to the problem Solver DLL provides different optimization routines to obtain the best results. The Solver DLL Platform includes for example a Quadratic Solver extension to its Simplex-based Solver for linear programming problems. This LP/Quadratic Solver easily handles "efficient portfolio" models, using the Markowitz or Sharpe methods. For smooth nonlinear problems a Generalized Reduction Gradient (GRG) algorithm is implemented. Solver DLL provides furthermore Hybrid Evolutionary algorithms and algorithm for integer and mixed integer problems.

A.3 EXAMPLE PROBLEMS

The software survey has been conducted using three test problems. The problems used are shown below.

Problem 1:

$$\min \quad f(x) = (x_1 - 1)^2 + (x_1 - x_2)^2 + (X_3 - 1)^2 + (x_4 - 1)^4 + (x_5 - 1)^6$$

$$\text{subject to} \qquad x_1^2 \cdot x_4 + \sin(x_4 - x_5) - 2 \cdot \sqrt{2} = 0$$

$$x_2 + x_3^4 \cdot x_4^2 - 8 - \sqrt{2} = 0$$

with a used start point (2,2,2,2,2)

Problem 2:

min $f(x) = e^{x_1 \cdot x_2 \cdot x_3 \cdot x_4 \cdot x_5}$

subject to $x_1^2 + x_2^2 + x_3^2 + x_4^2 + x_5^2 = 10$

$x_2 \cdot x_3 - 5 \cdot x_4 x_5 = 0$

$x_1^3 + x_2^3 = -1$

$-2.3 \le x_i \le 2.3$ i = 1,2

$-3.2 \le x_i \le 3.2$ i = 3,4,5

with a used start point (-2,2,2,-1,-1)

Problem 3:

max $f(x) = -5 \cdot x_1 - \frac{5000}{x_1} - 20 \cdot x_2 - \frac{72000}{x_2} - 10 \cdot x_3 - \frac{144000}{x_3}$

subject to $1 - \frac{4}{x_1} - \frac{32}{x_2} - \frac{120}{x_3} \ge 0$

$1.E-5 \le x_i$ i = 1,2,3

with a used start point (100,100,100)

A.4 EASE OF USE

This section gives a description of the user friendliness, the handbook and the implementation possibilities with other programs for each of the evaluated optimization packages. Furthermore, the possibilities to analyze the optimization will be examined and a rating over all criteria will be performed. The rating uses a scale from 1 to 10, where 10 describes the best and 1 the worst.

A.4.1 LINGO

Lingo has a very user-friendly interface. It is extremely easy to enter objective and constraint functions. Lingo accepts equality and inequality constraints, the later ones in positive null form as well as in negative null form. All calculation with Lingo could be easily done and no optimization solver parameters needed to be modified to get results. During this evaluation no obvious downside was found considering the user friendliness. Therefore, Lingo is rated with a 10 in this category.

Lingo has an online help function that gives a lot of examples for different problems. However, the help is sometimes not detailed enough to answer a question, especially concerning problems involving interfaces with other programs. For this reasons, the handbook is rated as 8.

Lingo offers a possibility to call self-written programs for calculating the objective and constraint functions. Lingo also provides the possibility to be called from other programs to start an optimization. Due to time constraints and insufficient

documentation, this feature has not been tested during this evaluation. An estimated rating for the interaction with other programs is 6.

Lingo has no post processing capabilities. At the end of an optimization a solution report is created. This report contains information about the found optimum, the value of the objective function and the step in which the solution has been found. Since the user has no way in getting more information, this feature is insufficient and is rated with a 4.

A.4.2 MATLAB

The user interface for an optimization in MATLAB is one command line. This command line specifies all necessary information and is therefore not very user friendly. However, once it is understood how to enter the optimization problem correctly, it is more convenient to enter one line than to enter half a page of code to get an optimization running. Therefore, the user friendliness is rated as a 6.

MATLAB offers an online help that is also available as a PDF document for easy print out. The documentation is very thorough and gives plenty examples for a better understanding of the useable functions. The only downside is the difficulty to navigate through the handbook, especially finding the section that applies to the given problem. This results in a rating of 8 for the user handbook.

Since MATLAB has its own programming language with easy programmable interfaces to other languages, the implementation of an optimization in other programs can be very easily done. Thus, the interaction with other programs is rated as a 10.

For optimization, no special post processing tools are provided but MATLAB offers a great variety of possibilities for displaying function and values. Therefore, post-processing capabilities can be self-programmed within limitations. These limitations are defined by the output of the optimization program. MATLAB gives, for example, no information about the values of the design variables for each iteration step. Instead the calculated function value is given with the value of the constraint that is most strongly violated. This is not enough information to plot detailed post processing graphs. For this reasons, the post processing capabilities are rated with 5.

A.4.3 NLPQL

NLPQL does not have a user interface. To define an optimization problem the user needs to modify FORTRAN source code and compile it. This is even necessary if different start values are chosen for the optimization. This is very inconvenient and the user friendliness is therefore rated with 3.

A handbook was not available for this evaluation. The documentation in the source code is short and insufficient to understand how to use the program correctly. This causes the user to do some trial and error runs before a problem can be solved. For this reason, the handbook is rated with 1.

The implementation possibilities of NLPQL with other programs are almost unlimited. Since the program is available in its source code, modification to call other programs can be easily done. Even non FORTRAN programs can be called using a batch

script and using ASCII files for the data exchange. This results in a rating of 10 for this category.

NLPQ has no post processing capabilities. However, since it is possible to write out all required data in each step it is possible to write a batch script plotting all interesting values. Therefore, the post-processing capabilities are rated with 3.

A.4.4 EPOGY

At the first look, Epogy seems to be a very user-friendly program. During the evaluation, however, problems occurred which took time to solve. For example, it is necessary to follow a specific order in steps to define the input and output variables in the proper input and output files. Otherwise, the input and output files could not be found and the variables could not be defined. Furthermore, the output provided by Epogy includes many design points, but gives no clear indication as to which is the optimum. The user has to check the optimization history on his own, to figure out at which iteration the best solution occurred. This results in a rating of 4 for the user friendliness.

The handbook of Epogy is very thorough and detailed and has two tutorials to learn how to use the program. Unfortunately, it is not able to overcome the shortcomings of the program and is therefore to some extent useless, since the average user will get stuck in the beginning of the handbook. The handbook is rated with 6.

Epogy is designed to use all kind of analysis programs to run an optimization. It writes an input file with the values of the design variables and starts the analysis program that reads the input file. The analysis program reads these values, does the analysis, and

writes out an output file with the new values of the design variables. This principle allows building an arbitrary long chain of analysis programs to run an optimization. This is in general a good idea and therefore rated with 8.

Epogy has a good post processing module. The objective function and the constraint functions can be plotted as well as the design variables. It is also possible to plot geometry with the right specifications during the definition phase. Therefore, the post processing is rated with a 9.

A.4.5 OPTDESX

OptdesX has a very user friendly environment. All parameters can be defined within the OptdesX program package. However, problems occurred in converging to an optimal solution running the example problems. After manipulation of some parameters it was possible for OptdesX to converge and print the solution. Other difficulties using OptdesX can occur during the linking phase of the user program with OptdesX. During this evaluation however, no problems occurred and the user friendliness of OptdesX is therefore ranked as 7.

OptdesX has a detailed handbook including three tutorials to learn how to use the program. It also has sections for all areas of the program, so that it can be easily used for reference when questions occur. For this reasons the handbook is rated with an 8.

OptdesX provides an easy interface to combine analysis programs with the optimization routine. The linking is done by a FORTRAN program, which can call other

FORTRAN or non-FORTRAN programs to do the calculation. The evaluation showed no problems in this area and is therefore ranked with a 10.

The post processing module of OptdesX is very good. It is possible to display all kinds of plots and matrices. It is, for example, possible to plot the objective function, the constraint functions and the design variables. It is also possible to show the gradients for each step of the optimization. Since no weak points could be found for the post processing module, it is rated as 10.

A.4.6 VISUALDOC

VisualDOC has an excellent user interface. Similar to OptdesX, all parameters can be defined within the program. The user has different possibilities to provide analysis programs, which can be executables, MATLAB m-files or Visual Script files. Visual Script is based on the same idea as Epogy. The user can define the sequence in which analysis programs will be run and define the values which need to be read out of the output files. This allows a great variety of possibilities and makes it easy to build an optimization setup. For this reasons the user friendliness of VisualDOC is rated with 10.

VisualDOC is delivered with a good documentation package. The documentation has a couple of tutorials depending on the optimization method, sections for all areas of the program and a good description how to use Visual Script. Working with the handbook during this evaluation was useful and the handbook is therefore rated with 9.

The great variety of possible programs and languages makes it very easy to implement analysis programs into VisaulDOC. The implementation for the example

programs has been done through MATLAB m-files and went without any problems. For this reasons, the implementation possibilities for user analysis programs are rated with 10.

The post processing capabilities of VisualDoc are excellent. It is possible to plot the objective function, the constraint functions and the design variables for each iteration step. The only negative point is, information about the gradients cannot be displayed. For this reasons, the post processing capabilities are rated with 9.

A.4.7 SOLVER DLL

Solver DLL has an insufficient user interface. Even after extensive study of the manual and several Email contacts with the user support it was not possible to get one example problem to run. Therefore all categories are ranked with 1 and Solver DLL will not be further considered in this survey.

A.5 RESULTS OF THE EXAMPLE PROBLEMS

This section gives an overview over the results for each of the example problems. A list for all three problems with all values of the design variables, objective and constraint values is presented in table A.2 to A.4. For comparability the constraint functions are converted, so that the right side is equal to zero.

To be able to compare the quantitative and the qualitative data a raking for each problem is done. This allows at the end to find the best optimization program.

Table A.2 Complete list for problem 1

Problem 1						
	Lingo	Matlab	NLPQL	Epogy (SQP)	OptdesX	VisualDOC
X1	1.166172	1.166195551	1.1654204	1.1624871	1.165233	1.167769
X2	1.182111	1.182152257	1.1784916	1.1121664	1.178693	1.190257
X3	1.380257	1.380266606	1.3806693	1.3914846	1.380421	1.381353
X4	1.506036	1.506011631	1.5054691	1.4940523	1.50599	1.502901
X5	0.6109196	0.61097359	0.60487835	0.56118733	0.6054863	0.6098839
F(X)	0.241504917	0.241505097	0.241528891	0.248912833	0.241522775	0.241570464
Const 1	-8.36837E-07	-2.61181E-07	2.08474E-06	-6.07089E-03	-2.26314E-06	2.27867E-05
Const 2	-4.40940E-06	-3.88522E-07	1.30501E-05	6.64065E-02	-1.23212E-05	-2.57545E-05
Iterations	4	20	17	N/A	20	17

Table A.3 Complete list for problem 2

Problem 2						
	Lingo	Matlab	NLPQL	Epogy	OptdesX	VisualDOC
X1	-1.717143	-1.717104094	-1.7178433	-1.7171401	-1.716971	-1.716329
X2	1.595709	1.595663977	1.5965452	1.60E+00	1.59551	1.594763
X3	1.827247	1.827319099	1.82592	1.8272909	1.827567	1.828748
X4	-0.7636423	-0.763647466	-0.7635668	-0.76136702	-0.7634682	-0.7590436
X5	-0.7636439	-0.763647466	-0.7635668	-0.76136702	-0.7638567	-0.768517
F(X)	0.053949852	0.053949849	0.053949016	0.054881974	0.05394972	0.053938073
Const1	4.62496E-07	-5.74081E-09	-5.45848E-06	-6.46849E-03	3.46498E-06	1.39076E-04
Const2	5.62238E-07	-2.05056E-09	-7.47873E-06	1.76106E-02	-7.48647E-08	-2.69905E-04
Const3	-2.26657E-07	1.09571E-09	1.93539E-04	7.97764E-04	1.14437E-06	-2.52868E-05
Itearations	27	6	5	N/A	12	31

Table A.4 Complete list for problem 3

Problem 3						
	Lingo	Matlab	NLPQL	Epogy	OptdesX	VisualDOC
X1	55.33629	55.33632277	55.346332	49.047058	55.27334	55.3779
X2	87.88748	87.88747561	87.854839	82.690613	87.97341	87.96232
X3	212.9121	212.912122	212.95829	226.48569	212.7772	212.7863
F(X)	-5749.473428	-5749.473642	-5749.473999	-5772.364641	-5749.259777	-5749.555221
Const1	-8.29687E-08	-1.55431E-15	2.33393E-09	1.62620E-03	-8.40915E-05	3.08058E-05
Itearations	64	13	31	N/A	11	11

A.5.1 PROBLEM 1

Figure A.1 shows the optimum of objective function found by the different optimization programs for the first example problem. Since the goal of the optimization was to minimize the objective, lower values are better.

One can see that most optimization programs are identical for the first three significant numbers. Only the solution found by Epogy shows a relevant difference from the solution found by the other programs. On a smaller scale one can see that Lingo and MATLAB found the lowest objective function values for this problem. To determine if a found solution is valid it must be in compliant with it constrains. Figure A.2 shows the value of the constraint functions at the optimum for each optimization program.

Const 1 and Const 2 describe the first and the second constraint given in problem 1. As one can see almost all solutions have a deviation less then 5.E-05, which should be good enough for most real life problems. Only the solution found by Epogy differs by 6.E-02, which is substantial to the minimum. On a smaller scale, it is visible that the solutions found by Lingo MATLAB and OptdesX show the smallest deviation from the constraints.

A ranking for the best objective and the lowest deviation from the constraints for problem 1 has been done. Table A.5 shows the values for each optimization program.

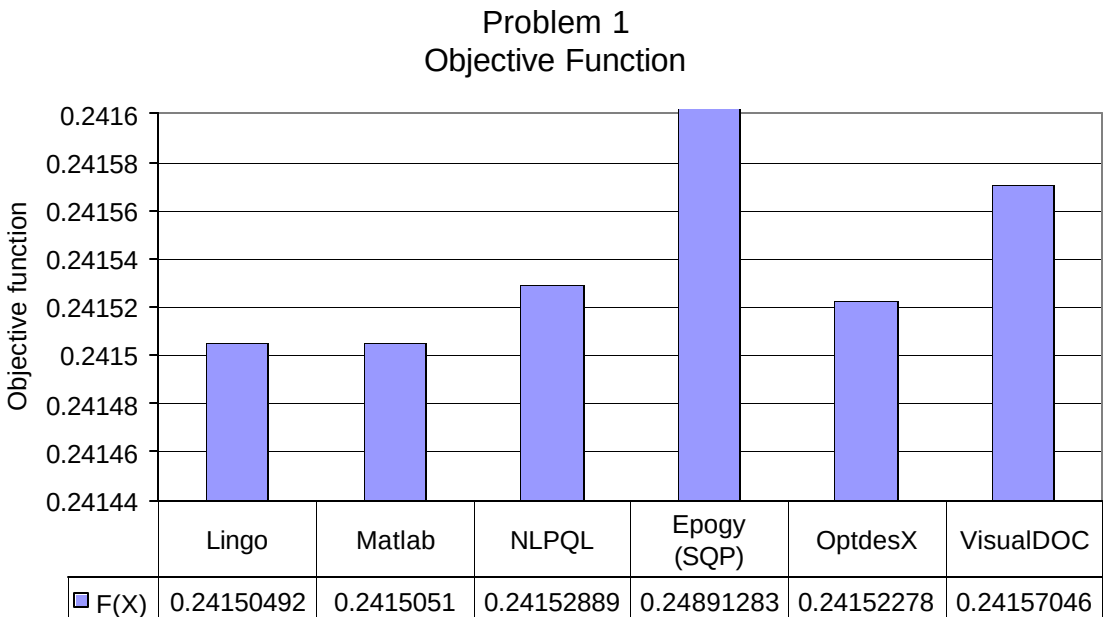

Figure A.1 Objective function problem 1

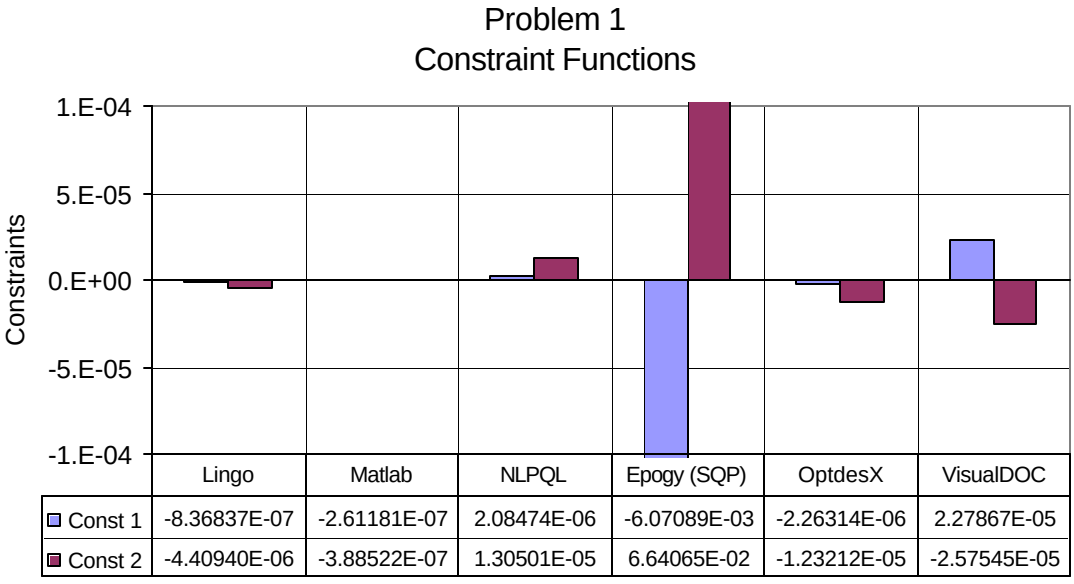

Figure A.2 Constrained function problem 1

Table A.5 Ranking for problem 1

Ranking	Lingo	MALAB	NLPQL	Epogy	OptdesX	VisualDOC
Objective	10	10	6	2	8	5
Constraints	9	10	8	2	9	8

A.5.2 PROBLEM 2

Figure A.3 shows the optimum of objective function found by the different optimization programs for the second example problem. The goal of this optimization was again to minimize the objective function. Thus, lower values show a better result.

It is again visible that most of the solutions are identical for the first three significant digits. Only the solution found by Epogy differs again significant from the solutions found by the other optimization programs. The solutions found for this problem are almost identical for Lingo, MATLAB, NLPQL and OptdesX; only VisualDOC has an objective function value which is slightly lower than the ones from the other optimizations.

FigureA.4 shows the value of the constraint functions for the solutions found for problem 2. As one can see Lingo MATLAB and OptdesX show an excellent accordance with the constraints. The solution found by NLPQL has a deviation of constraint three, which is in the order of 2E-04 and substantial compared to the objective function value. The solution found by VisualDOC shows deviation for all three constraints in the order of 2E-04. This is again a high value and a not sufficient solution. The solution found by Epogy shows an even bigger deviation and is also not sufficient for an optimization.

A ranking for the best objective and the lowest deviation from the constraints for problem 2 has been done. Table A.6 shows the values for each optimization program.

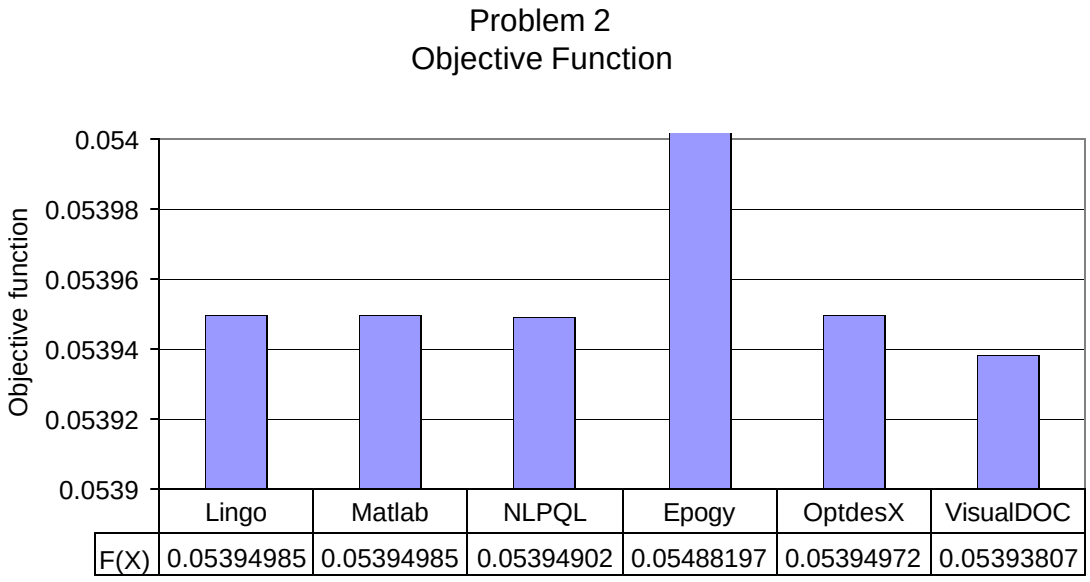

Figure A.3 Objective function problem 2

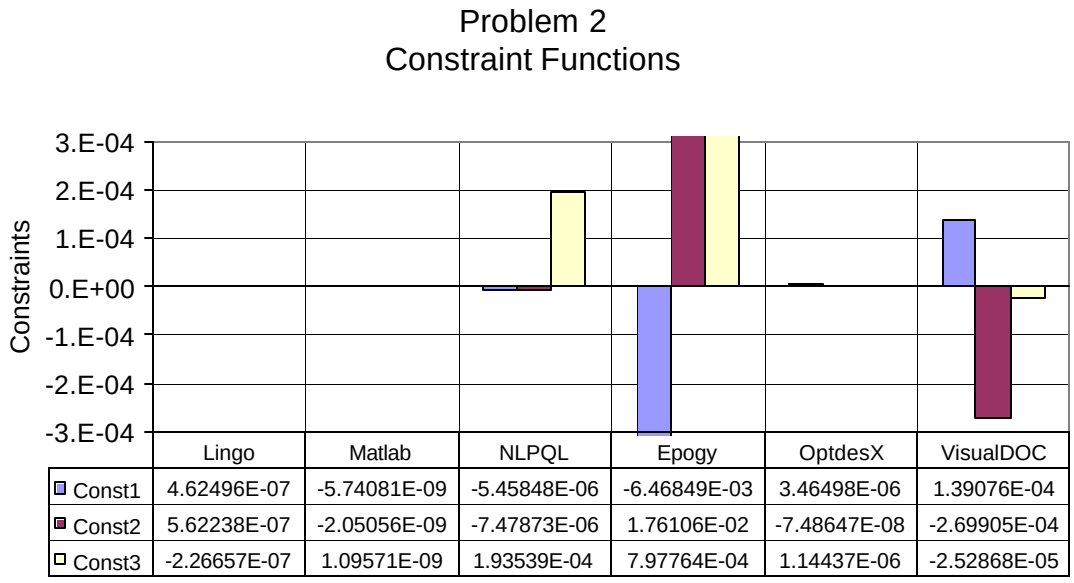

Figure A.4 Constrained function problem 2

Table A.6 Ranking for problem 2

Ranking	Lingo	MALAB	NLPQL	Epogy	OptdesX	VisualDOC
Objective	9	9	9	2	9	10
Constraints	9	10	7	2	9	5

A.5.3 PROBLEM 3

Figure A.5 shows the optimum of objective function found by the different optimization programs for the third example problem. The goal of this optimization was to maximize the objective function. Thus, higher values show a better result. For easier comparability the y-axes has been reversed.

On can see that most solutions are identical for the first four significant digits. Again, Epogy has a significantly lower value for the solution compared with the solutions of the other optimization programs. The difference between Lingo, MATLAB, NLPQL, OptdesX and VisualDOC is negligible compared to the value of the objective function.

Figure A.6 shows the value of the constraint functions for the solutions found for problem 3. It is visible that Lingo, MATLAB and NLPQL have an excellent correspondence with the constraints. OptdesX and VisualDOC show a deviation in the order of 5E-05, which is small compared to the value of the objective function and probably sufficient for most real life applications.

Another ranking for the best objective and the lowest deviation from the constraints for problem 3 has been done. Table A.7 shows the values for each optimization program.

A.6 SUMMERY

For a summery the quantitative ratings and the qualitative ratings are added and an average is built. Since each example problem has been rated on its own, a bigger emphasis is put on the results of the optimization since the rating of the results is over

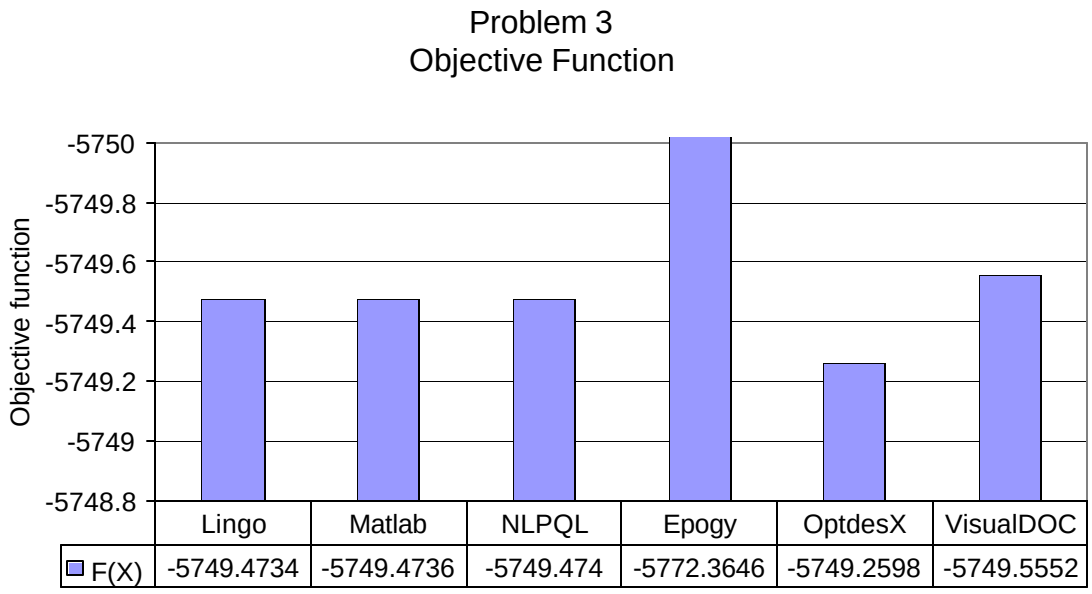

Figure A.5 Objective function problem 3

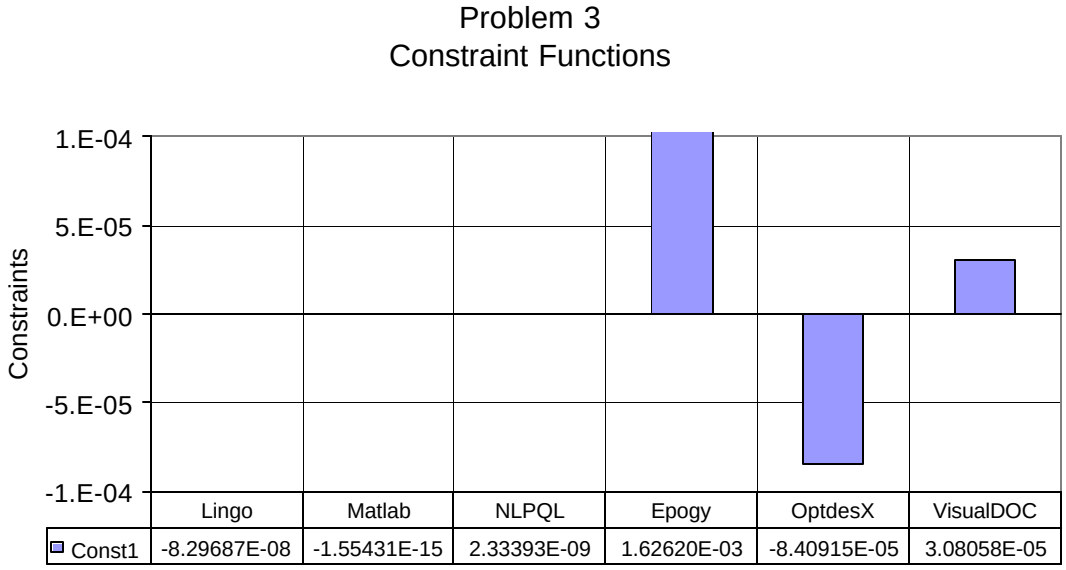

FigureA.6 Constrained function problem 3

Table A.7 Ranking for problem 3

Ranking	Lingo	MALAB	NLPQL	Epogy	OptdesX	VisualDOC
Objective	9	9	9	2	10	8
Constraints	10	10	10	2	5	8

represented in the calculation. Table A.8 shows the summarized rankings and the average.

It is visible that Lingo, MATLAB and OptdesX show the best overall performance. NLPQL shows good results for the optimization, but the average rating for ease of use is low so that the total rating is lower then of the other optimization programs. Visual DOC has intermediate ratings for the results of the optimization, but shows excellent performance in ease of use. The Epogy program package has just an average rating for the usage and shows a poor performance in the optimization results.

A.7 RECOMMENDATION

Since MATLAB, NLPQL and OptdesX are already available at the University it is recommended to purchase either Lingo or VisaulDOC as another optimization program. One of the biggest plus points for Lingo is the price of $320 for 200 non-linear design variables. The disadvantage of Lingo is the combination with other analysis programs, which could not be tested during this survey.

The advantage of VisualDoc is exactly the weak point of Lingo. VisualDOC has an excellent interface to other programs, which makes it easy to build an optimization. However, with $750 for an annual license it is more expensive then Lingo and did not show as good optimization results.

Table A.8 Summarized ratings

Rating of	Lingo	MATLAB	NLPQL	Epogy	OptdesX	VisualDOC
User friendliness	10	6	3	4	7	10
Handbook	8	8	1	6	8	9
Implementation	6	10	10	8	10	10
Post processing	4	5	3	9	10	9
Objective (1)	10	9	9	2	8	6
Constraints (1)	10	10	6	2	8	5
Objective (2)	9	9	9	2	9	10
Constraints (2)	9	10	7	2	9	5
Objective (3)	9	9	9	2	10	8
Constraints (3)	10	10	10	2	5	8
Average	**8.5**	**8.6**	**6.7**	**3.9**	**8.4**	**8**

VITA

Joachim Drenckhan was born in Johannesburg, South Africa on September 20, 1974. From 1977 he lived and was raised in Hamburg, Germany, where he went to elementary and high school. He graduated from “Gymnasium Dörpsweg” 1994. From there, he went to the University of Applied Sciences in Hamburg, Germany and graduated 2001 as a “Diplom Ingenieur”. He was furthermore selected for the “Walter Blohm” award as the best student of the graduation class 2001. In the same year he went to the University of Tennessee Space Institute in Tullahoma, which was funded by a Fulbright Scholarship. He transferred 2002 to the University of Tennessee, Knoxville where he received a Master of Science in aerospace engineering with a minor in mathematics.

Joachim is currently pursuing his doctorate in mechanical engineering at the “Universität der Bundeswehr” in Hamburg, Germany.